ATOMIC-RESOLUTION CHARACTERIZATION OF ACTIN-BINDING PROTEIN, COFILIN-2, IN COMPLEX WITH TWO NUCLEOTIDE-STATES OF F-ACTIN, BY MAGIC ANGLE SPINNING NMR SPECTROSCOPY

by

Jenna B. Yehl

A dissertation submitted to the Faculty of the University of Delaware in partial fulfillment of the requirements for the degree of Doctor of Philosophy in Chemistry and Biochemistry

Fall 2016

ProQuest LLC.
789 East Eisenhower Parkway
P.O. Box 1346
Ann Arbor, MI 48106 – 1346

ATOMIC-RESOLUTION CHARACTERIZATION OF ACTIN-BINDING PROTEIN, COFILIN-2, IN COMPLEX WITH TWO NUCLEOTIDE-STATES OF F-ACTIN, BY MAGIC ANGLE SPINNING NMR SPECTROSCOPY

by

Jenna B. Yehl

Approved: _____
Murray Johnston, Ph.D.
Chair of the Department of Chemistry and Biochemistry

Approved: _____
George H. Watson, Ph.D.
Dean of the College of Arts and Sciences

Approved: _____
Ann L. Ardis, Ph.D.
Senior Vice Provost for Graduate and Professional Education

I certify that I have read this dissertation and that in my opinion it meets the academic and professional standard required by the University as a dissertation for the degree of Doctor of Philosophy.

Signed: _____

Tatyana Polenova, Ph.D.
Professor in charge of dissertation

I certify that I have read this dissertation and that in my opinion it meets the academic and professional standard required by the University as a dissertation for the degree of Doctor of Philosophy.

Signed: _____

Dmitri Kudryashov, Ph.D.
Member of dissertation committee

I certify that I have read this dissertation and that in my opinion it meets the academic and professional standard required by the University as a dissertation for the degree of Doctor of Philosophy.

Signed: _____

Murray Johnston, Ph.D.
Member of dissertation committee

I certify that I have read this dissertation and that in my opinion it meets the academic and professional standard required by the University as a dissertation for the degree of Doctor of Philosophy.

Signed: _____

Colin Thorpe, Ph.D.
Member of dissertation committee

ACKNOWLEDGMENTS

During my time at the University of Delaware and in the Polenova laboratory I have been fortunate to work and collaborate with many talented scientists. All of these people have greatly impacted me as a person as I pursued my doctoral degree. I will acknowledge them below.

To my research advisor, Dr. Tatyana Polenova, I am grateful for this opportunity to work with you during my doctoral studies. I am thankful for Dr. Polenova for providing me all the resources and opportunities to conduct this research. Her guidance and insight has challenged me to be a better scientist and more importantly guided me to be a critical thinker.

I would like to thank my committee members, Dr. Murray Johnston, Dr. Colin Thorpe, and Dr. Dmitri Kudryashov from the University of Delaware and the Ohio State University for their time and constructive input during my doctoral studies. Your input and suggestions are invaluable and helped guide me throughout my studies.

To our collaborators, Dr. Dmitri Kudryashov and Dr. Elena Kudryashova at the University of Ohio, it is with my sincerest appreciation for your time and input in my doctoral work. This project would not be possible if it weren't for this collaboration. I especially want to thank Dmitri for his valuable insight and expertise into this project.

To Dr. Gaungjin Hou, I am greatly appreciative for your time and guidance while in the Polenova laboratory. Your patience and willingness to help with NMR experiments was invaluable to my success during my time here.

To the post-docs in the Polenova laboratory, Dr. Rupal Gupta, Dr. Caitlin Quinn, and Dr. Xingyu Lu. Thank you for your willingness to teach and share your wisdom about chemistry, NMR and life. My time in the Polenova Lab was greatly impacted by having you as mentors.

To Mingyue, it is with sincere appreciation for your friendship and continual support during my time in Delaware. You have always been there to offer encouragement and help whenever I was in need. I am sincerely grateful to have a friend like you while in this lab.

To the people in the Polenova lab, Si, Chris, Rupal, Cait, Xingyu, Manman, Changmiao, Maple, Matt, Ting, Wenfei, Jodi, Ryan and Vera, you have greatly impacted my time here at Delaware. Thank you for your continual support and encouragement.

To my former research advisors, Dr. David Rovnyak and Dr. Timothy Strein from Bucknell University, thank you for inspiring me to continue my education and thank you for your continued mentorship during my time here at Delaware.

To my family and friends, thank you. I am forever grateful for your love and support during this time. I am truly blessed to have each of you in my life.

TABLE OF CONTENTS

LIST OF TABLES

LIST OF FIGURES

LIST OF ABBREVIATIONS

2D	Two-dimensional
3D	Three-dimensional
ABP	Actin-binding protein
ADP	Adenosine diphosphate
ATP	Adenosine triphosphate
CORD	Combined R2nv-driven
CSI	Chemical shift index
DARR	Dipolar assisted rotational resonance
dREDOR	Double rotational echo double resonance
EM	Electron microscopy
F-actin	Filamentous actin
FID	Free induction decay
G-actin	Globular actin
HETCOR	Heteronuclear correlation
HSQC	Heteronuclear single quantum correlation
MAS	Magic angle spinning
MINT	Maximum entropy Interpolation
NOESY	Nuclear Overhauser effect spectroscopy
NMR	Nuclear magnetic resonance
NUS	Non-uniform sampling
PAIN-CP	Proton assisted insensitive nuclei cross polarization
PAR	Proton-assisted recoupling
PDB	Protein data bank
PDSD	Proton driven spin diffusion
REDOR	Rotational echo double resonance
RFDR	Radio frequency driven recoupling
SDS-PAGE	Sodium dodecyl sulfate polyacrylamide gel electrophoresis
SD1	Subdomain-1
SD2	Subdomain-2
SD3	Subdomain-3
SD4	Subdomain-4
SSNMR	Solid-state nuclear magnetic resonance
TALOS	Torsion angle likelihood obtained from shift and sequence similarity

TEDOR	Transferred echo double resonance
TEM	Transmission electron microscopy
TMR	Tetramethyrodamine maleimide
TPPI	Time proportional phase incremation
TPPM	Two-pulse phase modulation decoupling

ABSTRACT

Cofilin, an actin-binding protein, is critical for actin dynamics within the cell. Actin dynamics are responsible within the cell for many essential cellular processes such as cell motility, cell division and endocytosis. Cellular processes are related via actin-binding proteins and the nucleotide state of F-actin. Actin polymerization/depolymerization and filament severing have been extensively studied via X-ray fibre diffraction and cryo-electron microscopy; however, atomic-level structural information of actin associated proteins assembled on F-actin remained inaccessible.

Here we report the first atomic-level resolution characterization of cofilin-2 assembled with F-actin in two nucleotide states (F-actin-ADP and F-actin-ADP-BeFx), by high-resolution magic-angle-spinning NMR. We have characterized the intermolecular interface of cofilin-2 on actin filaments in two nucleotide states. The results revealed remarkable spectral resolution enabling in-depth characterization of these systems. The MAS NMR approach presented here establishes the foundation for atomic-resolution structural analysis of a broad range of actin-associated proteins assembled on F-actin.

Chapter 1

ACTIN AND ACTIN-BINDING PROTEINS

The eukaryotic cytoskeleton system is composed of three types of protein filaments: microtubules, intermediate filaments and actin filaments. (Figure 1.1) These cytoskeletal filaments perform a variety of essential functions within eukaryotic cells such as cell motility, cell division, intracellular transport, and signal transduction. Actin is a highly conserved, abundant, and functionally versatile protein expressed in virtually all eukaryotic cells. Actin plays an essential role in cellular division, cellular motility and mechanical support through its interactions of over 100 actin-binding proteins (ABPs).[1] Cofilin, an actin-binding protein, is involved in the cellular dynamics of actin by accelerating the turnover of actin filaments.[2] Involvement of the actin depolymerizing factor (ADF)/cofilin family of ABPs has been associated with various pathologies such as Hinaro bodies, neurodegenerative disease, Williams syndrome and ischemic kidney disease.[2] Despite the recent efforts to investigate actin-binding proteins, such as cofilin, mechanistic information is still not fully understood at the atomic-level.

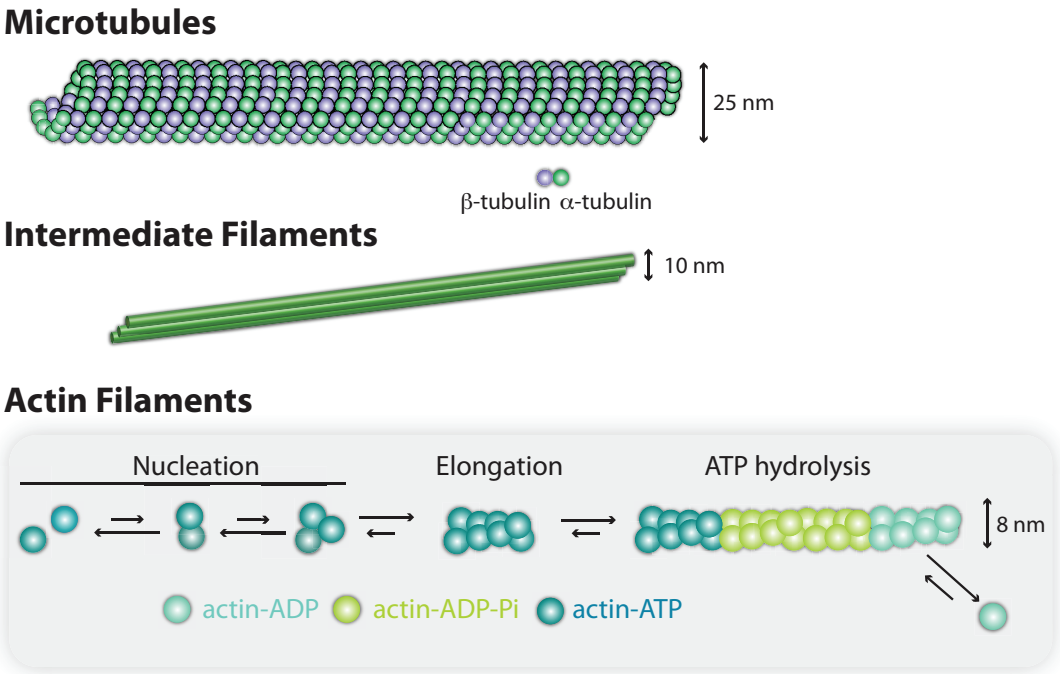

Figure 1.1: Cytoskeletal filaments (top) microtubules composed of α-tubulin and β-tubulin heterodimers, (middle) intermediate filaments and (bottom) actin filaments showing actin nucleation, elongation and the ATP hydrolysis of actin filaments. Actin-ADP monomers are colored in light blue, actin-ADP-Pi monomers are colored in green and Actin-ATP monomers are in cyan.

Within the last decade X-ray fibre diffraction and cryo-electron microscopy (cryo-EM) have made progress in understanding the structure of actin filaments and the interaction of actin filaments with actin-binding proteins. However, atomic-level structural information of actin-associated proteins assembled on F-actin has not been yet accessible. Magic-angle spinning (MAS) NMR studies reported here yielded atomic-resolution information on the 3D structure of human cofilin-2 assembled on the F-actin interface. In this dissertation, we focused on cofilin-2 and will be referred to as "cofilin" throughout this thesis.

1.1 Structure of F-actin

Actin can exist in two states within the eukaryotic cell, globular actin (G-actin) (Figure 1.2) and fibrous actin (F-actin). Globular actin is a 43-kDa actin monomer that is comprised of two domains, a larger or inner domain and a small or outer domain. The large domain consists of subdomains 1 and 2 (SD1, 2) and the small domain consists of subdomains 3 and 4 (SD3, 4). A nucleotide (ATP or ADP) with a tightly bound divalent cation (Mg^{2+} under physiological conditions) is positioned deep inside the cleft between SD2 and SD4 and is clamped between two phosphate binding loops, P1 and P2 (Figure 1.3).

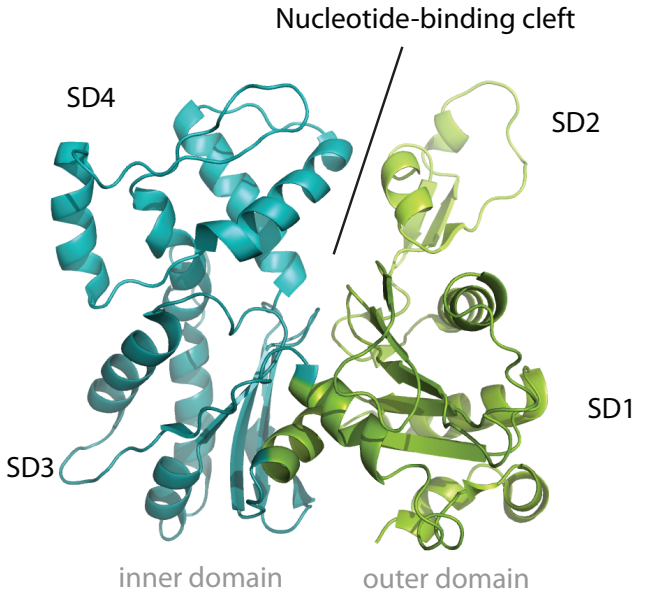

Figure 1.2: Globular actin (G-actin) structure (PDB: 2BTF). The small or outer domain is shown in green. The subdomains of the outer domain are labeled subdomain 2 (SD1) and subdomain 2 (SD2). The subdomains of the inner domain are shown in blue. The subdomains of the inner domain are labeled subdomain 3 (SD3) and subdomain 4 (SD4). The nucleotide-binding cleft is shown on the G-actin structure.

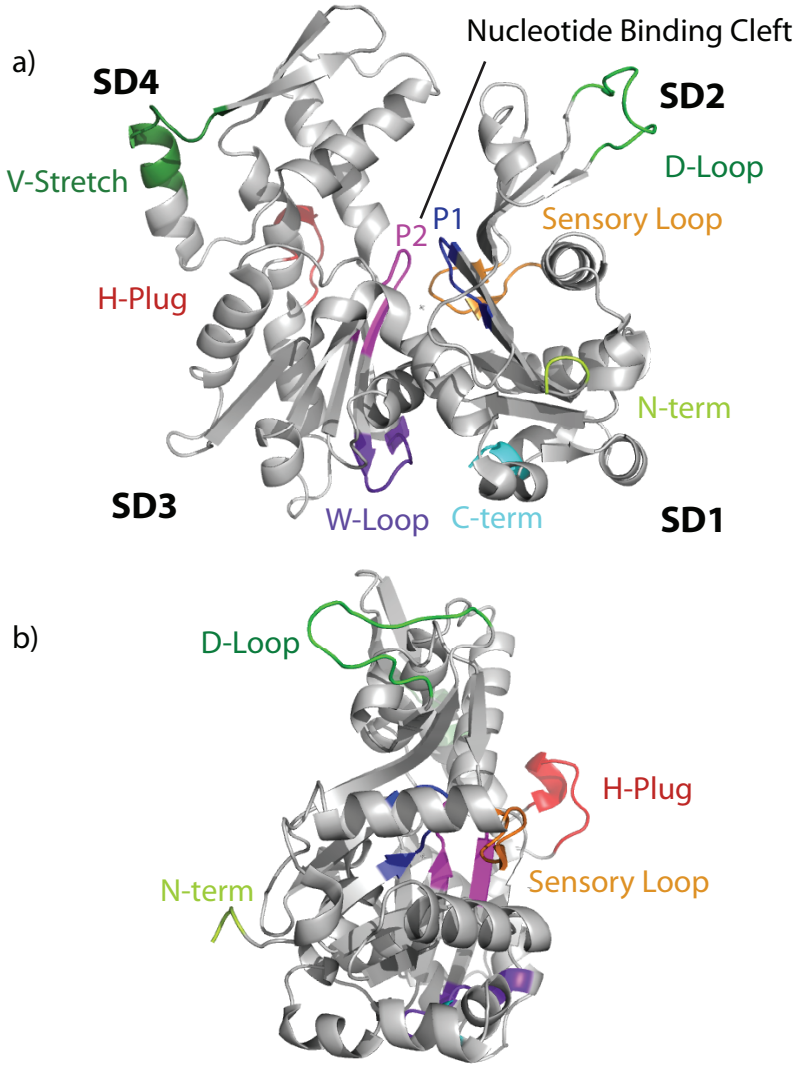

Figure 1.3: The G-actin structure shown in two different projections. The phosphate binding loops P1 (residues 11-16) and P2 (residues 154-161) are in dark blue and magenta, respectively. The sensory loop (residues 70-78) is shown in orange and the H-plug (residues 264-271) is in red. The D-loop (residues 40-51) is colored in light green and the W-loop (residues 165-172) is in purple. The V-stretch (residues 227-237 is in green and the N- and C-terminal regions are colored in yellow and cyan, respectively.

The structure of actin filaments and actin filament treadmilling are formed by an ATP-dependent assembly of G-actin monomers. Actin filaments organize into a polymer-like structure composed of G-actin subunits. The filaments polymerize into a right-handed, two-chained long helix of 13 G-actin monomer repeats every six turns in an axial distance of 35.9 nm.[3] (Figure 1.4)

During the last decade, X-ray fibre diffraction and cryo-EM have made progress in determining the structure of actin filaments. The first near-atomic resolution structure of F-actin was determined by combining X-ray fibre diffraction data and the crystal structure of G-actin.[4] In this model the G-actin subunit was used to determine the structure of actin filaments. It is known that the G-actin monomer changes conformations upon F-actin polymerization. Oda et al have studied the nature of the G- to F-actin transition using X-ray fibre diffraction.[5] It is reported that the main component of the transition from the G- to F-actin is a 20° propeller-like rotation of the outer domain with respect to the inner domain about an axis roughly at right angle to the helix axis.[5] Subdomains 2 and 4 also undergo a bending movement in the same direction. This propeller-like rotation causes the actin monomer to flatten upon polymerization and the DNase-1 binding loop (D-loop) to adopt an open-loop conformation and insert itself into the target binding cleft of the subunit immediately above it.

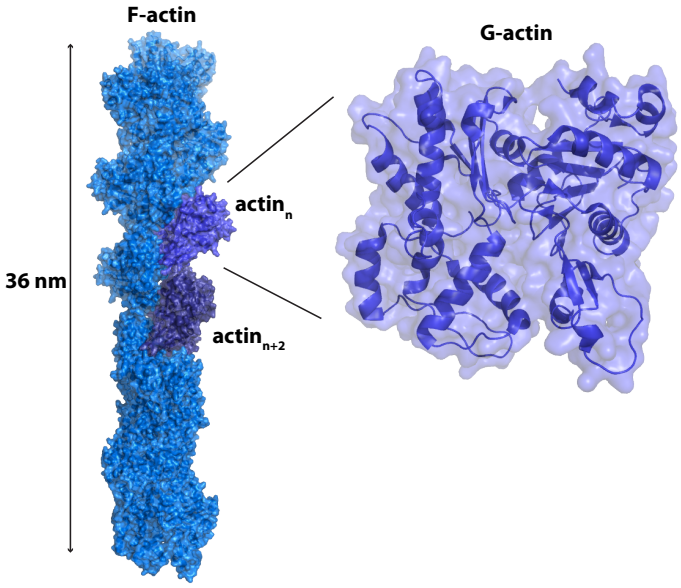

Figure 1.4: The helical structure of F-actin derived from cryo-EM. The G-actin molecules are arranged on a single helix with 13-G-actin monomer repeats. The G-actin monomer is shown on the right. Adjacent actin protomers are colored in purple and labeled n and n+2.

Cryoelectron microscopy has also been used to study the structure of actin filaments. Atomic models of F-actin of have been reported by Fujii et al.[6] The cryo-EM model of F-actin derived in this study is very similar to that inferred from the X-ray fibre diffraction, with the most significant difference found in the DNase-1 binding loop, where the extension of the D-loop was observed to directly interact with the binding cleft of SD1 and SD3.[6] Despite the fact that significant insights were gained into the structure of F-actin from these models to help understand processes such as cell motility, atomic-level information about nucleotide dependent states of F-actin and actin in the presence of actin-binding proteins (ABPs) is still needed.

1.1.1 Nucleotide States of Actin Filaments

The interaction of actin with nucleotides is an essential part of actin polymerization. ATP binds to G-actin and is hydrolyzed to ADP and Pi upon actin polymerization. G-actin alone has been reported to have ATPase activity but upon polymerization the ATPase activity is increased by a factor of 40,000.[7] Within the filament the release of the inorganic phosphate is about two orders of magnitude slower than the hydrolysis and results in the newly assembled part of the filaments to be composed mostly of ADP-Pi protomers (Figure 1.5). Older filaments are mainly comprised of ADP-protomers. The ADP-Pi and ATP nucleotide states of actin protomers of actin filaments are structurally very similar[8] and are more structurally stable than ADP-F-actin.[9] ADP-F-Actin filaments have been reported to be less structurally stable due to the intra- and intermolecular conformational rearrangements in the filament as the result of the inorganic phosphate release. These conformational changes result in ADP-F-actin filaments forming more flexible structures.[10]

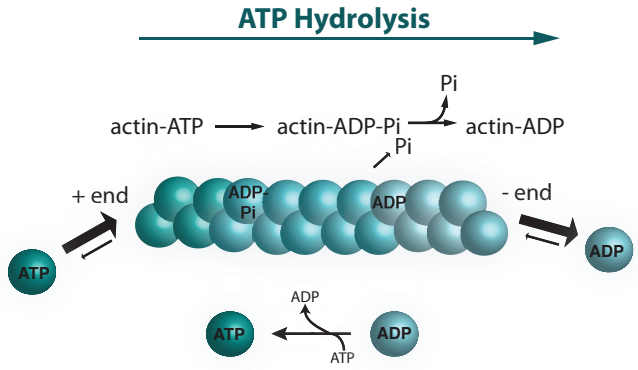

Figure 1.5: The hydrolysis of ATP in actin filaments.

The ATP hydrolysis of actin filaments results in functionally polar actin filaments with the ADP-F-actin end (minus or pointed end) and at the location of actin protomers disassembly. The disassembly of ADP-G-actin protomers from the actin filaments supplies G-actin subunits that undergo an exchange of ADP to ATP before adding to the opposite filament end (plus or barbed end), Figure 1.6. This process is known as actin treadmilling and is for cell migration, invasion and endo- and exo-cytosis. It has been shown with nonhydrolyzable analog, AMP-PNP, that ATP hydrolysis is not required for polymerization.[11,12]

Nucleotide hydrolysis of F-actin is one of the main factors regulating the transition between G- and F-actin; however, within the cell, actin treadmilling is accelerated and regulated by various actin-binding proteins. Most of these actin-binding proteins preferentially bind to one of the nucleotide-related conformational states of actin.[13] Preferential binding for nucleotide specific states can be observed in actin-binding proteins, such as cofilin and profilin. Conformation changes in actin protomers upon polymerization have been studied using X-ray crystallography, biochemical methods, and molecular modeling. The nucleotide-dependent conformational states of actin have been reported, in which G-actin was found to adopt an open or closed nucleotide binding cleft conformation. Crystallographic evidence in actin monomers cocrystallized with actin-binding proteins, Arp2/3, an actin-related protein of the Arp2/3 nucleation complex, supported the observation of more open conformations in the ADP- compared with the ATP-state of actin. Over 80 actin-binding proteins have been cocrystallized with actin monomers and are found to be in a tightly closed state in the presence of actin monomers in the ADP and ATP nucleotide states.[3] Among the crystal structures of G-actin cocrysallized with actin-

binding proteins, four have been reported for G-actin in the absence of actin-binding proteins. Two of these structures were solved in the presence of ADP and a ATP-like AMP-PNP-state, and polymerization was prevented by labeling the C374 residue with tetramethyrodamine maleimide (TMR).[14,15] The other two structures were solved in the ADP and ATP states of actin, and polymerization was blocked by a site-directed mutagenesis of two residues that play a very important role in the longitudinal contacts between the SD3 and SD4. Interestingly, in both ADP states of the uncomplexed actin reported to have closed states on the nucleotide binding cleft, nucleotide-dependent conformational rearrangements near the sensory loop were proposed to translate into structural changes in the actin molecule. Structural differences observed in the DNase-binding loop (D-loop), WH2-binding loop (W-loop) and the N- and C-terminal ends of actin play a very important role in the regulation of conformational changes of F-actin and the recognition of actin-binding proteins to the nucleotide dependent states of actin filaments.

1.2 Actin-Binding Proteins

Within the cell, the assembly and disassembly of actin filaments and the organization of higher order networks is regulated by over 100 actin-binding proteins. Actin-binding proteins are involved in processes such as nucleation, filament growth and stability, regulation of F-actin assembly and disassembly and regulation of higher-order F-actin structures. Aside from actin-binding proteins playing crucial roles in actin dynamics these are involved in physical support or track within the cell.

1.2.1 Nucleation of Actin Filaments

Nucleation of actin filaments plays an important role in the process of polymerization. In the process of polymerization, nucleation is the rate limiting step. Actin-binding proteins that promote nucleation filaments such as Arp2/3 complex nucleate actin monomers into stable G-actin trimers that acts as the nucleus for filament growth. Arp2/3 binds to the pointed-end and promotes rapid growth from its barbed end. Along with Arp2/3 proteins, formin proteins also participate in filament nucleation. The regulation of filament growth once nucleated monomers are formed is controlled by capping proteins, e.g. gelsolin and tensin, which block the addition of new monomers.

1.2.2 Stabilization of Actin Filaments

In addition to nucleating filaments, stabilizing filaments is also a critical process within the cell. Tropomyosins bind along the filament and stabilize the filament against spontaneous depolymerization. Tropomyosins inhibit the binding of depolymerizing proteins such as actin depolymerizing factor (ADF)/cofilin proteins and gesolin. Tropomyosin also plays an important role in regulating the interaction of myosin with the actin filament in striated muscle.

1.2.3 Polymerization and Depolymerization

Depolymerization and polymerization of actin filaments is an important process in actin treadmilling that is essential for cell motility and cell division. The process of depolymerization is driven by the actin-depolymerizing factor/cofilin family of proteins. These proteins bind to the sides of aged filaments of the ADP-F-actin and the result in filament severing that is important for the acceleration of filament treadmilling.

1.2.4 Higher-Order Actin Structures

Along with the actin-binding proteins that are associated with the dynamic processes of actin filaments above, actin-binding proteins also help regulate and form higher-order F-actin structures. Higher order structures, such as F-actin bundling and F-actin crosslinking are crucial for the overall shape and order in the cell. The formation of tight actin bundles is found to take place in microvilli while loosely ordered structures are found in actin stress fibers. Actin-binding proteins that promote actin crosslinking belong to the flexible dimeric filamin or tetrameric spectrin proteins.

In the cytoskeleton, actin also acts as mechanical framework for physical support and transport. This involves actin-binding proteins facilitating the interconnection between actin to membranes or membrane proteins and actin to other cytoskeletal elements. Annexin proteins play an important role in linking actin to microtubules, intermediate filaments and, in some cases, actin to both microtubules and intermediate filaments.

1.3 Function of Cofilin, An Actin-Binding Protein

The ADF/cofilin family of actin-binding proteins play a key role in actin dynamics and is essential for all eukaryotic cells. This family of proteins is expressed in all eukaryotes with three forms in mammals: ADF, cofilin-1 (non-muscle tissue), and cofilin-2 (muscle tissue). Cofilin-1 is the most ubiquitous and most widely studied protein from this family.

ADF/cofilins are the best-known regulators of actin filaments and play a crucial role in the non-equilibrium assembly/disassembly of actin filaments. The regulation of assembly and disassembly of actin filaments is based on the relative concentration of cofilin to actin within the cell and the relative concentration of cofilin

to other actin-binding proteins.[16] In low ratios of cofilin/actin (<1/100 of the K_D), persistent filament severing is observed.[17] In contrast, cofilin stabilizes actin filaments at high cofilin/actin ratios.[18] At higher ratios of cofilin/actin cofilin can also be responsible for nucleating filaments. Severing of action filaments occurs at low ratios and this can accelerate polymerization at newly formed ends. (Figure 1.6).

1.3.1 Deactivation/Activation of Cofilin

The activation and deactivation of cofilin is regulated by the phosphorylation of Ser3. There are two families of ubiquitous kinases that are responsible for the inactivation of cofilins by phosphorylation. LIM (Lin-11, Isl1, and Mec-3) kinases (LIMK) and testicular kinases regulate cofilin activity by phospohorylation.[19,20] Phostphatases of the Slingshot (SSH) family and haloacid dehalogenase phosphatase chronophin (CIN) enzymes work to reactivation phosphorylated cofilin.[21] It has been recently reported that cofilin is also regulated by phosphorylation of S23 and/or 24.[22]

1.3.2 Modulation of Cofilin Activity by pH

The ability of cofilin to sever actin filament is pH dependent. Within the cell the physiological range of pH can change (6.8-7.4).[23] Changes in pH can modulate the severing ability of cofilin to depolymerize actin filaments. Cofilin's pH-dependency has been previously studied and was found to have a greater sensitivity for filament severing than members of the ADF/cofilin family in vitro and in vivo. [24,25]

1.3.3 Modulation of Cofilin Activity by Actin-Binding Proteins

Cofilin's ability to depolymerize actin filaments as well as accelerate actin dynamics can be modified by the presence of other actin-binding proteins. Actin-interacting protein 1 (Aip1) is a protein that greatly enhances ADF/cofilin-induced

actin dynamics.[26,27] It was demonstrated that the local concentrations of Aip1 and cofilin-1 directly impact cell migration efficiency and play a very important role in the regulation of actin dynamics.[28,29]

As mentioned previously, tropomyosins modulate the ability of cofilin to sever actin filaments. Tropomyosins are rod shaped molecules that have the ability to span several actin subunits along the actin filament. This interaction stabilizes the actin filament and prevents cofilin from binding. Tropomyosins also prevent the filament-branching activity of the Arp2/3 complex.[30]

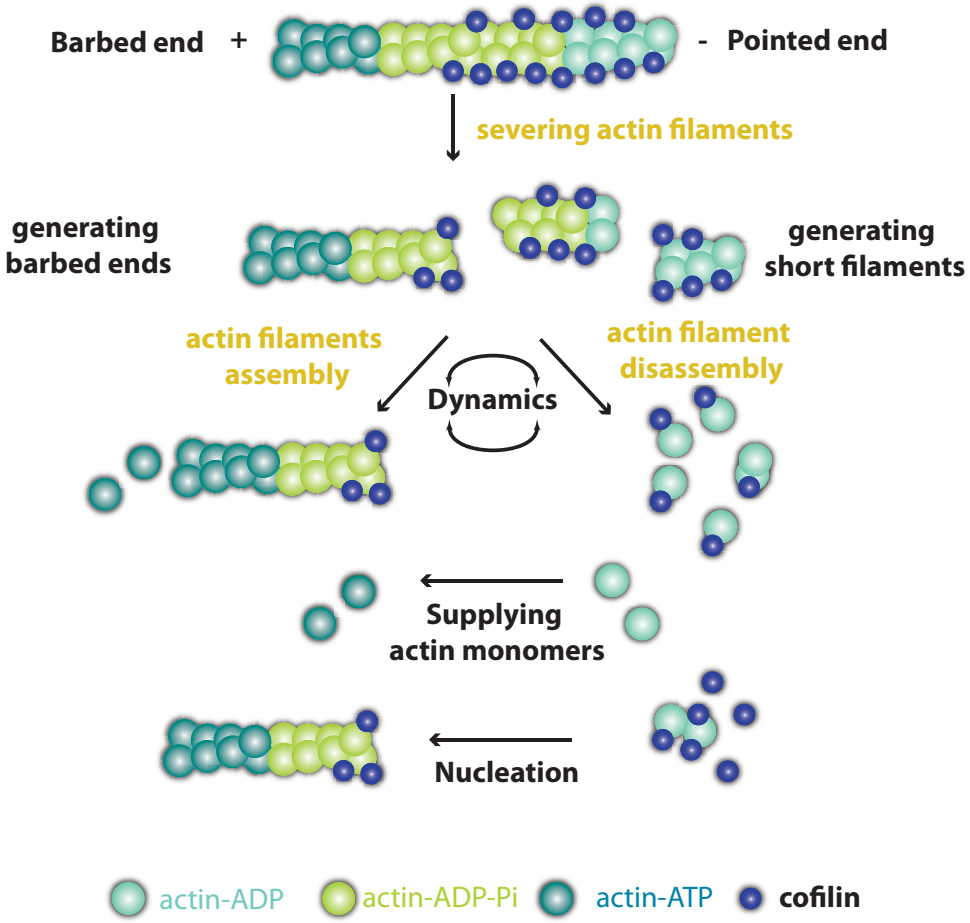

Figure 1.6: The assembly and disassembly of actin filaments in treadmilling via actin-binding protein, cofilin.

1.3.4 Cofilin-Actin and Disease

As discussed previously, the deactivation of cofilin occurs when Ser3 becomes phosphorylated. The deactivation of cofilin inhibits cofilin's ability to bind to actin and regulate the assembly/disassembly of actin filaments. At low ratios (<1:100) of cofilin to actin subunits, cofilin has the ability to nucleate filament growth or more

rapidly depolymerize filaments, depending on the amount of available actin monomers.[17] At higher ratios cofilin binding to actin filaments can stabilize a twisted form of actin, eliminating the phalloidin binding site and causing the actin filaments to bundle.[31]

Within the cell, high levels of stress cause depletion in ATP levels. Highly active cofilin is regulated by phosphatases (Slingshot family) and has preferential binding to ADP-actin. Cofilin phosphatases are activated as ATP levels decline under cellular stress.[32] As cofilin is activated the preferential binding to actin-ADP generates cofilin-saturated ADP-actin filaments. These filaments in turn will aggregate to form rods. The formation of cofilin-actin rods have been observed in vivo and in vitro and serves as a protective function under stress conditions by limiting ATP consumption due to actin treadmilling.[33,34]

Within neurons, cofilin is involved in postsynapitic remodeling. Cofilin-actin rods will form within neurites and cause synaptic dysfunction. The formation of cofilin-actin rods in the cases of cytoskeletal abnormalites and the loss of synaptic function are typical of sporadic Alzheimer Disease (AD).

REFERENCES

(1) Pollard, T. D.; Cooper, J. A. *Science* **2009**, *326*, 1208.

(2) Bobkov, A. A.; Muhlrad, A.; Shvetsov, A.; Benchaar, S.; Scoville, D.; Almo, S. C.; Reisler, E. *J. Mol. Biol.* **2004**, *337*, 93.

(3) Dominguez, R.; Holmes, K. C. *Annu. Rev. Biophys.* **2011**, *40*, 169.

(4) Holmes, K. C.; Popp, D.; Gebhard, W.; Kabsch, W. *Nature* **1990**, *347*, 44.

(5) Oda, T.; Iwasa, M.; Aihara, T.; Maeda, Y.; Narita, A. *Nature* **2009**, *457*, 441.

(6) Fujii, T.; Iwane, A. H.; Yanagida, T.; Namba, K. *Nature* **2010**, *467*, 724.

(7) Blanchoin, L.; Pollard, T. D. *Biochemistry* **2002**, *41*, 597.

(8) Belmont, L. D.; Orlova, A.; Drubin, D. G.; Egelman, E. H. *Proc. Natl. Acad. Sci. USA* **1999**, *96*, 29.

(9) Levitsky, D. I.; Pivovarova, A. V.; Mikhailova, V. V.; Nikolaeva, O. P. *FEBS J.* **2008**, *275*, 4280.

(10) Isambert, H.; Venier, P.; Maggs, A. C.; Fattoum, A.; Kassab, R.; Pantaloni, D.; Carlier, M. F. *J. Biol. Chem.* **1995**, *270*, 11437.

(11) Cooke, R. *Biochemistry* **1975**, *14*, 3250.

(12) Cooke, R. *J. Biochem.* **1975**, *3*, 146.

(13) Bugyi, B.; Carlier, M. F. *Annu. Rev. Biophys.* **2010**, *39*, 449.

(14) Otterbein, L. R.; Graceffa, P.; Dominguez, R. *Science* **2001**, *293*, 708.

(15) Graceffa, P.; Dominguez, R. *J. Biol. Chem.* **2003**, *278*, 34172.

(16) Van Troys, M.; Huyck, L.; Leyman, S.; Dhaese, S.; Vandekerkhove, J.; Ampe, C. *Eur. J. Cell Biol.* **2008**, *87*, 649.

(17) Andrianantoandro, E.; Pollard, T. D. *Mol. Cell. Biochem.* **2006**, *24*, 13.

(18) Pollard, T. D.; Cooper, J. A. *Science* **2009**, *326*, 1208.

(19) Scott, R. W.; Olson, M. F. *J. Mol. Med. (Berl)* **2007**, *85*, 555.

(20) Toshima, J.; Toshima, J. Y.; Takeuchi, K.; Mori, R.; Mizuno, K. *J. Biol. Chem.* **2001**, *276*, 31449.

(21) Huang, T. Y.; DerMardirossian, C.; Bokoch, G. M. *Curr. Opin. Cell Biol.* **2006**, *18*, 26.

(22) Sakuma, M.; Shirai, Y.; Yoshino, K.; Kuramasu, M.; Nakamura, T.; Yanagita, T.; Mizuno, K.; Hide, I.; Nakata, Y.; Saito, N. *Mol. Biol. Cell* **2012**, *23*, 3707.

(23) Pope, B. J.; Zierler-Gould, K. M.; Kuhne, R.; Weeds, A. G.; Ball, L. J. *J. Biol. Chem.* **2004**, *279*, 4840.

(24) Bamburg, J. R.; Wiggan, O. P. *Trends Cell Biol.* **2002**, *12*, 598.

(25) Bernstein, B. W.; Painter, W. B.; Chen, H.; Minamide, L. S.; Abe, H.; Bamburg, J. R. *Cell Motil. Cytoskeleton* **2000**, *47*, 319.

(26) Iida, K.; Yahara, I. *Genes Cells* **1999**, *4*, 21.

(27) Rodal, A. A.; Tetreault, J. W.; Lappalainen, P.; Drubin, D. G.; Amberg, D. C. *J. Cell Biol.* **1999**, *145*, 1251.

(28) Li, J.; Brieher, W. M.; Scimone, M. L.; Kang, S. J.; Zhu, H.; Yin, H.; von Andrian, U. H.; Mitchison, T.; Yuan, J. *Nat. Cell Biol.* **2007**, *9*, 276.

(29) Rogers, S. L.; Wiedemann, U.; Stuurman, N.; Vale, R. D. *J. Cell Biol.* **2003**, *162*, 1079.

(30) Ono, S. *Int. Rev. Cytol.* **2007**, *258*, 1.

(31) McGough, A.; Pope, B.; Chiu, W.; Weeds, A. *J. Cell Biol.* **1997**, *138*, 771.

(32) Huang, T. Y.; Minamide, L. S.; Bamburg, J. R.; Bokoch, G. M. *Dev. Cell* **2008**, *15*, 691.

(33) Minamide, L. S.; Striegl, A. M.; Boyle, J. A.; Meberg, P. J.; Bamburg, J. R. *Nat. Cell Biol.* **2000**, *2*, 628.

(34) Minamide, L. S.; Maiti, S.; Boyle, J. A.; Davis, R. C.; Coppinger, J. A.; Bao, Y.; Huang, T. Y.; Yates, J.; Bokoch, G. M.; Bamburg, J. R. *J. Biol. Chem.* **2010**, *285*, 5450.

Chapter 2

MAGIC ANGLE SPINNING NMR OF PROTEIN ASSEMBLIES: BASIC INTRODUTION

2.1 MAS NMR Methods to Study Protein Assemblies

Solid-state NMR (SSNMR) in the last decade has emerged as a new approach to study protein structure in macromolecular assemblies that are not amenable to traditional techniques, such as X-ray crystallography and solution NMR. In this chapter, an introduction of the general protocol for three-dimensional protein structure determination by solid-state NMR will be discussed.

2.2 Three-Dimensional Structure Determination of Proteins by MAS NMR

In the last decade advancements in hardware and experimental methods have allowed solid-state NMR to emerge as a primary method to study macromolecular assemblies. Three-dimensional (3D) structures of amyloid fibrils[1-4], microcrystalline proteins[5-8], membrane proteins[9-13], and large protein assemblies[14] have been obtained by SSNMR (Figure 2.1). The general procedure for 3D protein structure determination is reviewed below.

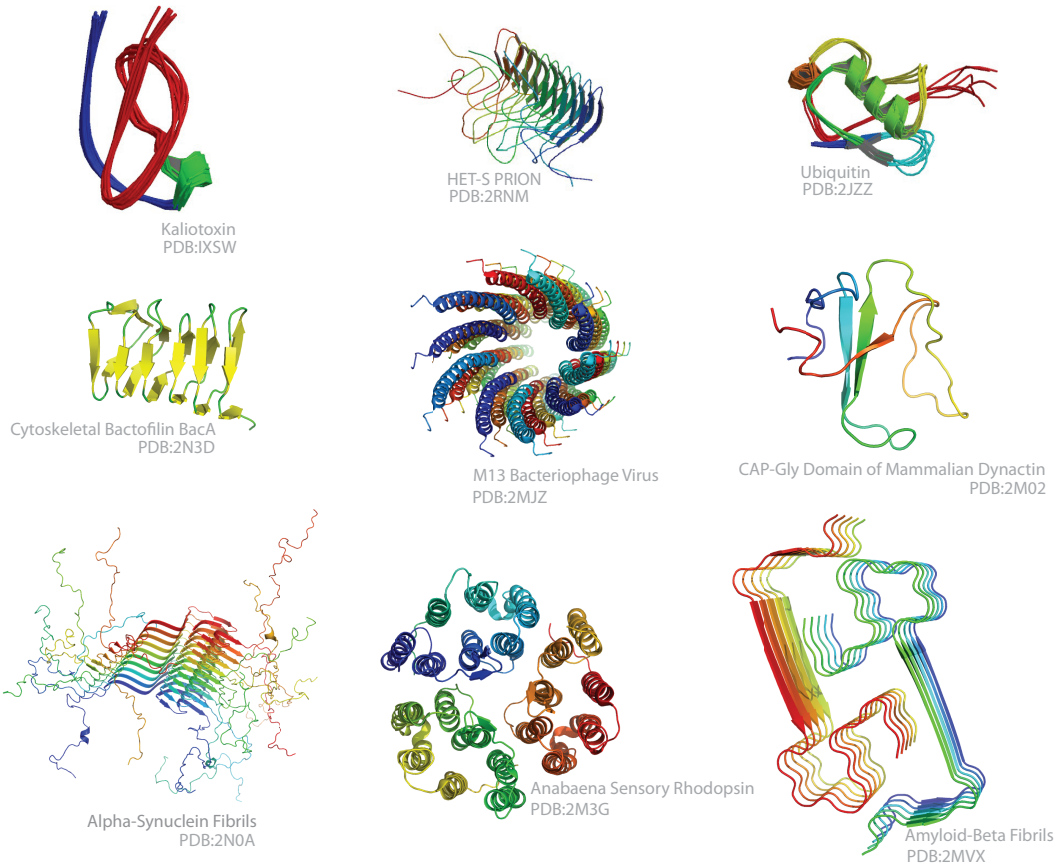

Figure 2.1: Protein structures solved by MAS NMR. Protein names and PDB codes are indicated by structure.

2.2.1 Resonance Assignments

The first and most time-consuming step of structure elucidation with SSNMR is site-specific resonance assignments. Typically, a protein contains thousands of carbon nuclei and hundreds of nitrogen nuclei. Resonance assignments is the process by which chemical shifts are attributed to specific atoms comprising the protein. Chemical shifts are sensitive to secondary structure, local electrostatic environment, hydrogen bonds, etc.

2.2.2 Multidimensional NMR Experiments for Resonance Assignments

In a one-dimensional NMR experiment, spectral overlap of signals prevents unambiguous assignments of protein nuclei. In order to resolve spectral overlap, two-dimensional and three-dimensional experiments can be used. Solid-state NMR employs a combination of homo- and heteronuclear dipolar-based spectra. The standard set of two-dimensional spectra that is required is NCA, NCO, NCACX, NCOCX, and DARR. In the NCACX spectrum, the amide nitrogen, alpha carbon, beta carbon, and other sidechain carbons within one amino acid (i) are observed in the spectrum (Figure 2.2).

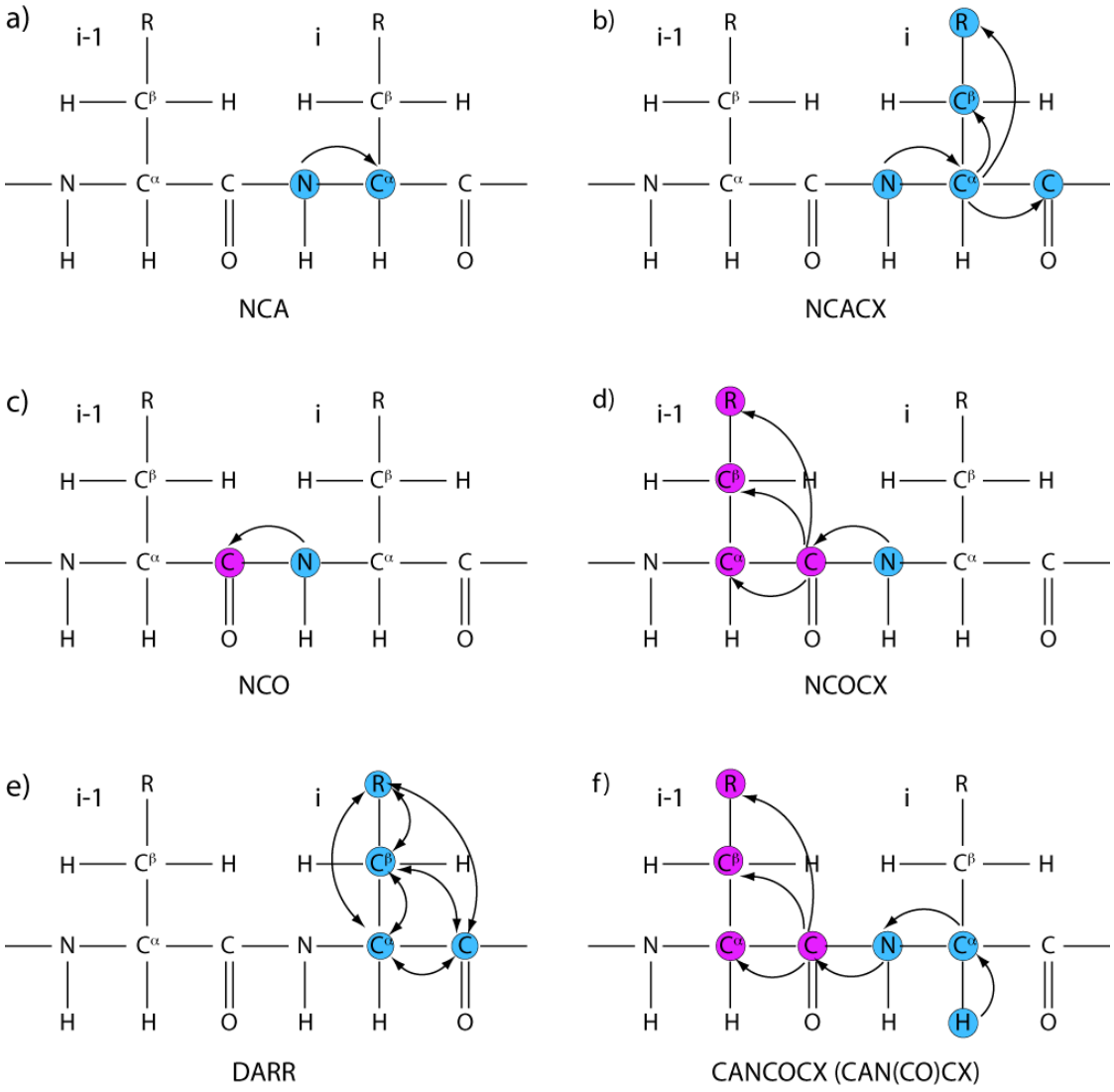

Figure 2.2: The magnetization transfer pathways in the dipolar-based MAS NMR experiments commonly used for resonance assignments (a) NCA, (b) NCACX, (c) NCO, (d) NCOCX, (e) DARR and (f) CANCOCX. The atoms involved in the magnetization pathways are colored in blue for residue i and in purple for residue i-1.

In the NCOCX spectrum, the amide nitrogen of residue i and the previous carbonyl carbon (i-1) and other carbons that are in close proximity of the residue i-1

are correlated. Since the amide nitrogen is connected to the alpha carbon of the i residue and the carbonyl carbon of residue i-1, heteronuclear (^{15}N-^{13}C) spectra will yield connectivity information for the protein polypeptide chain. For some small proteins, a high-quality set of two-dimensional spectra can yield full assignment with minimal spectral overlap and chemical shift degeneracies. For most proteins and protein assemblies, three-dimensional spectra will need to be collected. For 3D NCACX spectra, N-C-C correlations between the amide nitrogen, the alpha carbon, and side-chain carbons of residue i are observed. For 3D NCOCX spectra, the amide nitrogen of residue i and correlations between the alpha carbon and other carbons within the i-1 residue are observed. When performing resonance assignments, the nitrogen chemical shift and the carbon chemical shift of the particular amino acid will be aligned throughout all spectra. The protein backbone can be constructed by the alignment of all nitrogen, alpha carbons, carbonyl carbons and side-chain carbon chemical shifts throughout the other dimensions in the spectra.

Adding more dimensions to NMR experiments, better resolution can be gained. However, the experimental time increases dramatically with each added dimension. Other limitations, such as sample stability, instrument stability or limited spectrometer time can also limit the type of 3D experiment. With each dimension, a loss of magnetization transfer occurs. In solids, the magnetization transfer efficiency is 15% to 80%, and magnetization losses are compounded with each indirect dimension. This decrease in magnetization transfer will inherently affect the sensitivity of the NMR experiment.

2.2.3 Torsion Angle and Secondary Structure Predictions from Chemical Shifts

Once the chemical shifts assignments are completed for the protein, torsion angle and secondary information can be gained based on the chemical shifts of the backbone and sidechain atoms. The Chemical Shift Index (CSI)[15] can be used to predict secondary structure from chemical shifts but in calculating the tertiary structure of proteins, backbone torsion angles are needed. This dramatically improves the accuracy of the tertiary structure of the protein. One of the most widely used methods for backbone torsion angle prediction is TALOS+[16]. Using HN, H^{α}, C^{α}, C^{β}, C^{O}, and N chemical shifts, $TALOS^{+}$ is able to provide the Φ and Ψ backbone torsion angles for a given residue in the protein sequence.

2.2.4 Acquiring Restraints for Protein Structure Determination

Determining the tertiary structure of a protein requires several kinds of information. In addition to collecting datasets to obtain chemical shifts of protein residues, torsion angles, and secondary structure, the tertiary structure calculation needs a sufficient number of meaningful medium- and long-range distance restraints. These distance restraints are typically obtained from ^{13}C-^{13}C distances derived from spin diffusion experiments. Most common experiments are PDSD, DARR, PARIS, RDSD and CORD[5,7,12,17]. Along with homonuclear distance restraints gained from spin diffusion experiments, experiments are employed to derive homo- and heteronuclear ^{15}N-^{13}C, ^{13}C-^{13}C, ^{15}N-^{15}N, ^{1}H-^{1}H, distance restraints, such as CHHC/NHHC sequences for proton-mediated ^{13}C-^{13}C or ^{15}N-^{15}N correlations[18,19], proton-assisted recoupling (PAR) for ^{13}C-^{13}C/^{15}N-^{15}N correlations[20-22], proton-assisted insensitive nuclei cross polarization[23] (PAIN-CP), and transferred echo double resonance (TEDOR)[13].

Spin-diffusion experiments are the most information rich. In the ^{13}C-^{13}C spin diffusion experiments, the ^{13}C-^{13}C correlations observed are due to the dipolar coupling interaction between the nuclei. The dipolar interaction is proportional to the inverse of the cube of the distance between two atoms; therefore, the intensity of the signal is related to the distance between two atoms albeit in a complex way.[24,25] Using the previously determined chemical shifts of carbon atoms, the distance between these two atoms can be qualitatively gauged from signal intensity of this peak and will yield an estimate of the distance between the two atoms. Typically, medium- and long-range distances can be obtained by increasing the mixing time of the spin-diffusion experiment. At longer mixing times, more ^{13}C-^{13}C correlations between carbon atoms less than 6 Å can be detected. At longer mixing times in uniformly ^{13}C enriched proteins, a high degree of spectral crowding is observed in the spectra. To resolve this challenge, alternative protein labeling techniques are employed. Due to the abundance of ^{13}C atoms in proteins, most labeling strategies are tailored for backbone and sidechain ^{13}C incorporation. There have been several sparse labeling methods that have been developed to using different carbon sources for the protein production. Two of the most common methods are with [2-^{13}C]-glycerol or [1,3-^{13}C]-glycerol as the sole carbon source in minimal media[26,27] and [1, 3-^{13}C]-glucose, [2-^{13}C]-glucose, or [1,6-^{13}C]-glucose[26-28] (Figure 2.3).

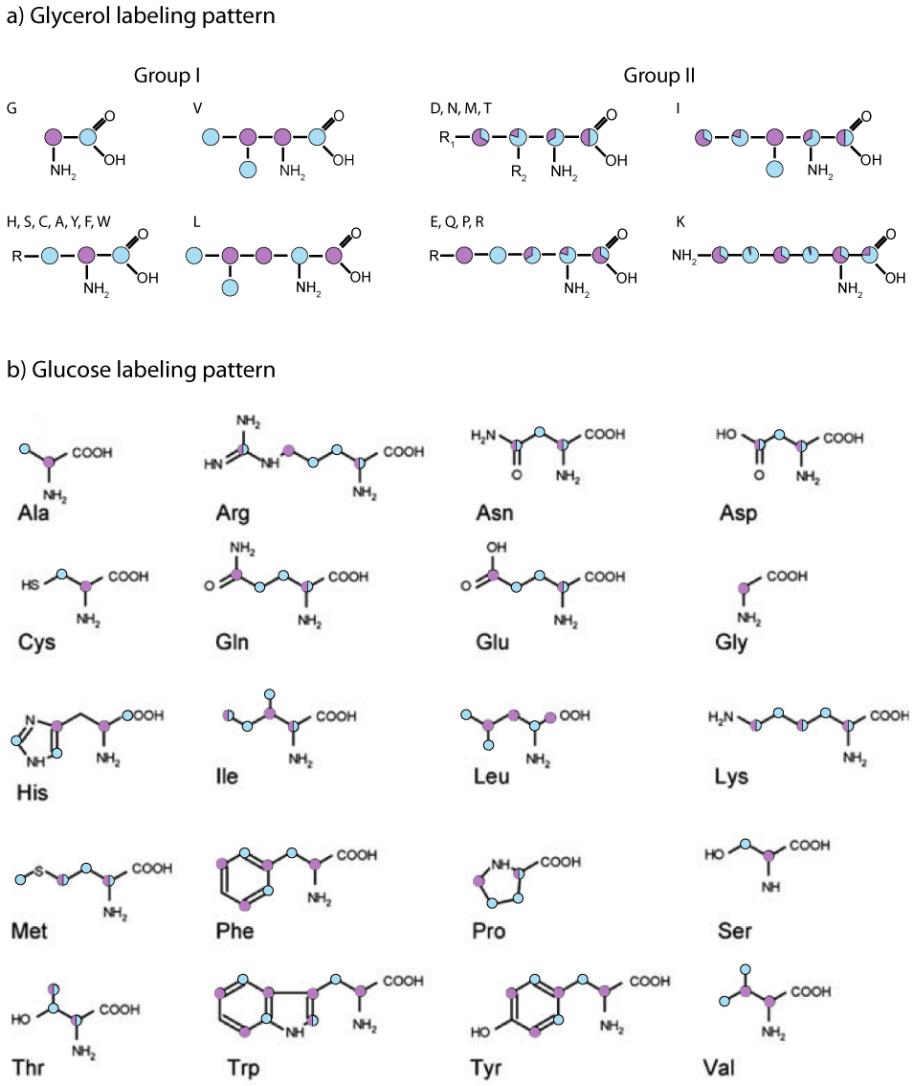

Figure 2.3: (a) The labeling patterns for each residue using [2-^{13}C]/[1,3-^{13}C]-glycerol and (b)[2-^{13}C/[1,6-^{13}C]-glucose. In (a) the purple dots represent the 13C sites that can be labeled by [2-^{13}C]-glycerol and the blue dots represent 13C sites that can be labeled by [1,3-^{13}C]-glycerol. In (b) the purple dots indicate the 13C sites that can be labeled by [2-^{13}C]-glucose and the blue dots indicate the ^{13}C sites that can be labeled by [1,6-^{13}C]-glucose. The dots filled completely and represented by a single color represent the ^{13}C sites that can be specifically labeled by one type of glycerol or glucose. In (a) and (b), the percentage of purple or blue color in each dot represents the possibility of the ^{13}C site that can be labeled by [2-^{13}C]-glycerol (purple) or [1,3-^{13}C]-glycerol (blue) in (a) and [2-^{13}C]-glucose (purple) and [1,6-^{13}C]-glucose (blue) in (b).

Sparse labeling in proteins reduce the amount of ^{13}C sites in proteins and dramatically simplify the spectra. Along with the simplification of spectra, the resolution is dramatically improved due to the removal of the majority of one-bond ^{13}C-^{13}C distance restraints.

2.2.5 Structure Calculation and Validation

In this step, the three-dimensional structure of the protein is determined. This is done computationally by a combination of molecular dynamics, experimental and chemical restraints to find the lowest energy protein structure. X-plor NIH is ubiquitously used to determine 3D protein structures from NMR restraints.[29,30] This program utilizes experimental restraints (distance restraints, vector angle restraints, CSA tensors, etc.) and chemical restraints in the geometric force field (chemical bonds, angles, dihedral angles, van der Waals force, etc.) to calculate a protein structure by minimizing the hybrid energy, using simulated annealing protocols.

2.3 Non-Uniform Sampling

In NMR experiments, points are typically collected equidistantly along the time-domain (Figure 2.4a). The distance between the points is the dwell time, which is dictated by the Nyquist theorem. For such linearly sampled data sets, fast Fourier Transform (FFT) from the data conversion between time- and frequency-domains. To encode the frequency-domain information, many fewer points are usually required than collected in a conventional, linear sampling method. Non-uniform sampling is an alternative to linear acquisition and do not require equidistant spacing between the data points.[31-34] NUS with appropriate sampling schedules permits to attain the information content, and either retain or increase time-domain sensitivity (for

equivalent experiment time) and lower the time cost of the overall experimental time; the latter particularly important for multidimensional experiments. [35-37] The work in our laboratory, in collaboration with the groups of Profs. David Rovnyak (Bucknell University) and Jeff Hoch (University of Connecticut), and others have established conditions where NUS based data collection of multidimensional MAS NMR spectra can permit sensitivity enhancements without the loss of resolution and for linear transformations between time- and frequency-domain, using Maximum Entropy Interpolation (MINT).[35-37] Some of these approaches are applied for the MAS NMR studies of cofilin/actin assemblies discussed in this thesis.

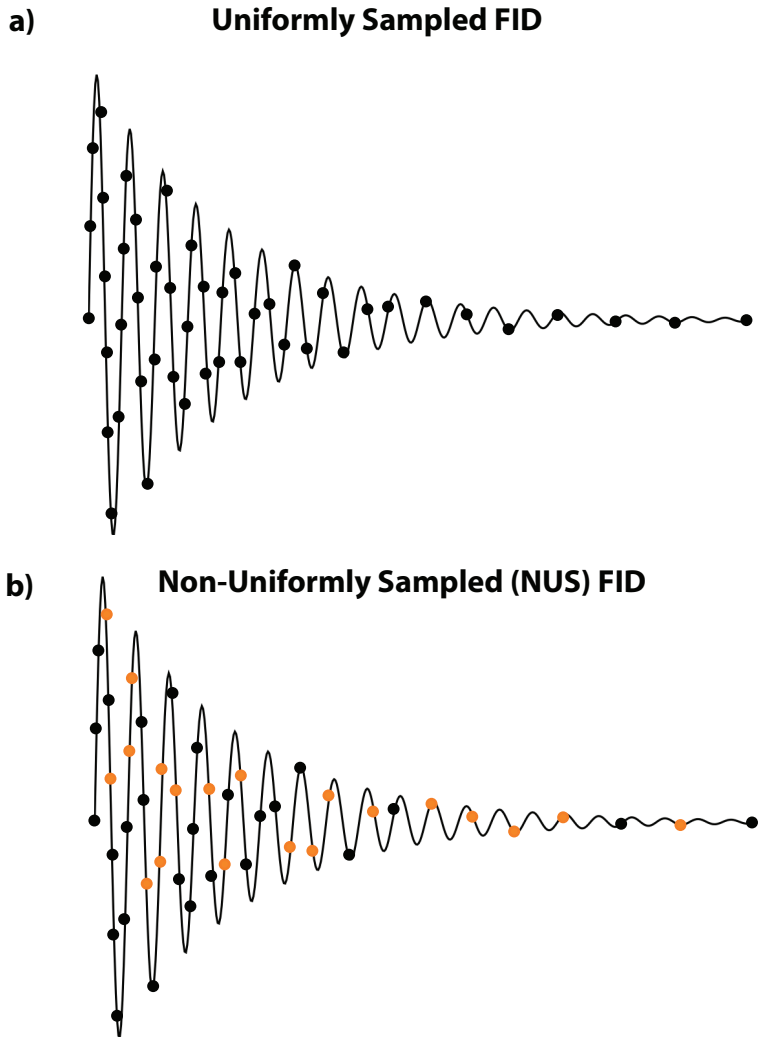

Figure 2.4: Free-induction decay (FID) of NMR signal. In (a) and (b), uniformly sampled data points are represented by black dots and data points that would be removed by non-uniform sampling (NUS) are colored in orange, respectively.

REFERENCES

(1) Jaroniec, C. P.; MacPhee, C. E.; Bajaj, V. S.; McMahon, M. T.; Dobson, C. M.; Griffin, R. G. *Proc. Natl. Acad. Sci USA* **2004**, *101*, 711.

(2) Iwata, K.; Fujiwara, T.; Matsuki, Y.; Akutsu, H.; Takahashi, S.; Naiki, H.; Goto, Y. *Proc. Natl. Acad. Sci. USA* **2006**, *103*, 18119.

(3) Nielsen, J. T.; Bjerring, M.; Jeppesen, M. D. *Angew. Chem. Int. Ed. Engl.* **2009**, *48*, 2118.

(4) Colvin, M. T.; Silvers, R.; Frohm, B.; Su, Y.; Linse, S.; Griffin, R. G. *J. Am. Chem. Soc.* **2015**, *137*, 7509.

(5) Castellani, F.; van Rossum, B.; Diehl, A.; Schubert, M.; Rehbein, K.; Oschkinat, H. *Nature* **2002**, *420*, 98.

(6) Etzkorn, M.; Martell, S.; Andronesi, O. C.; Seidel, K.; Engelhard, M.; Baldus, M. *Angew. Chem. Int. Ed. Engl.* **2007**, *46*, 459.

(7) Zech, S. G.; Wand, A. J.; McDermott, A. E. *J. Am. Chem. Soc.* **2005**, *127*, 8618.

(8) Franks, W. T.; Wylie, B. J.; Schmidt, H. L.; Nieuwkoop, A. J.; Mayrhofer, R. M.; Shah, G. J.; Graesser, D. T.; Rienstra, C. M. *Proc. Natl. Acad. Sci. USA* **2008**, *105*, 4621.

(9) Zhou, D. H.; Shea, J. J.; Nieuwkoop, A. J.; Franks, W. T.; Wylie, B. J.; Mullen, C.; Sandoz, D.; Rienstra, C. M. *Angew. Chem. Int. Ed. Engl.* **2007**, *46*, 8380.

(10) Balayssac, S.; Bertini, I.; Bhaumik, A.; Lelli, M.; Luchinat, C. *Proc. Natl. Acad. Sci. USA* **2008**, *105*, 17284.

(11) Loquet, A.; Bardiaux, B.; Gardiennet, C.; Blanchet, C.; Baldus, M.; Nilges, M.; Malliavin, T.; Bockmann, A. *J. Am. Chem. Soc.* **2008**, *130*, 3579.

(12) Manolikas, T.; Herrmann, T.; Meier, B. H. *J. Am. Chem. Soc.* **2008**, *130*, 3959.

(13) Nieuwkoop, A. J.; Wylie, B. J.; Franks, W. T.; Shah, G. J.; Rienstra, C. M. *J. Chem. Phys.* **2009**, *131*, 095101.

(14) Loquet, A.; Sgourakis, N. G.; Gupta, R. *Nature* **2012**, *486*, 276.

(15) Wishart, D. S.; Sykes, B. D. *J. Biomol. NMR* **1994**, *4*, 171.

(16) Shen, Y.; Delaglio, F.; Cornilescu, G.; Bax, A. *J. Biomol. NMR* **2009**, *44*, 213.

(17) Zhang, Y.; Doherty, T.; Li, J.; Lu, W.; Barinka, C.; Lubkowski, J.; Hong, M. *J. Mol. Biol.* **2010**, *397*, 408.

(18) Luca, A. C.; Mersch, S.; Deenen, R. *PLoS One* **2013**, *8*, e59689.

(19) Lange, A.; Luca, S.; Baldus, M. *J. Am. Chem. Soc.* **2002**, *124*, 9704.

(20) De Paepe, G.; Lewandowski, J. R.; Loquet, A.; Bockmann, A.; Griffin, R. G. *J. Chem. Phys.* **2008**, *129*, 245101.

(21) Lewandowski, J. R.; De Paepe, G.; Eddy, M. T.; Struppe, J.; Maas, W.; Griffin, R. G. *J. Phys. Chem. B* **2009**, *113*, 9062.

(22) Lewandowski, J. R.; De Paepe, G.; Eddy, M. T.; Griffin, R. G. *J. Am. Chem. Soc.* **2009**, *131*, 5769.

(23) Lewandowski, J. R.; De Paepe, G.; Griffin, R. G. *J. Am. Chem. Soc.* **2007**, *129*, 728.

(24) Grommek, A.; Meier, B. H.; Ernst, M. *Chem. Phys. Lett.* **2006**, *427*, 404.

(25) Manolikas, T.; Herrmann, T.; Meier, B. H. *J. Am. Chem. Soc.* **2008**, *130*, 3959.

(26) Hong, M.; Jakes, K. *J. Biomol. NMR* **1999**, *14*, 71.

(27) Hong, M. *J. Biomol. NMR* **1999**, *15*, 1.

(28) Lundstrom, P.; Teilum, K.; Carstensen, T.; Bezsonova, I.; Wiesner, S.; Hansen, D. F.; Religa, T. L.; Akke, M.; Kay, L. E. *J. Biomol. NMR* **2007**, *38*, 199.

(29) Schwieters, C. D.; Kuszewski, J. J.; Tjandra, N.; Clore, G. M. *J. Magn. Reson.* **2003**, *160*, 65.

(30) Clore, G. M.; Schwieters, C. D. *J. Mol. Biol.* **2006**, *355*, 879.

(31) Barna, J. C. J.; Laue, E. D.; Mayger, M. R.; Skilling, J.; Worrall, S. J. P. *J. Magn. Reson.* **1987**, *73*, 69.

(32) Barna, J. C. J.; Laue, E. D. *J. Magn. Reson.* **1987**, *75*, 384.

(33) Maciejewski, M. W.; Qui, H. Z.; Rujan, I.; Mobli, M.; Hoch, J. C. *J. Magn. Reson.* **2009**, *199*, 88.

(34) Rovnyak, D.; Frueh, D. P.; Sastry, M.; Sun, Z. Y. J.; Stern, A. S.; Hoch, J. C.; Wagner, G. *J. Magn. Reson.* **2004**, *170*, 15.

(35) Palmer, M. R.; Suiter, C. L.; Henry, G. E.; Rovnyak, J.; Hoch, J. C.; Polenova, T.; Rovnyak, D. *J. Phys. Chem. B* **2015**, *119*, 6502.

(36) Suiter, C. L.; Paramasivam, S.; Hou, G.; Sun, S.; Rice, D.; Hoch, J. C.; Rovnyak, D.; Polenova, T. *J. Biomol. NMR* **2014**, *59*, 57.

(37) Paramasivam, S.; Suiter, C. L.; Hou, G.; Sun, S.; Palmer, M.; Hoch, J. C.; Rovnyak, D.; Polenova, T. *J. Phys. Chem. B* **2012**, *116*, 7416.

Chapter 3

RESONANCE ASSIGNMENTS OF FREE COFILIN-2

3.1 Introduction

As discussed in Chapter 1, cofilin is a member of the actin-depolymerizing factor (ADF)/cofilin family of actin-depolymerizing proteins. The cofilin/ADF family of actin-binding proteins is essential for all eukaryotes and plays an extremely significant role in the regulation of actin dynamics in cell biology. Cofilin regulates the assembly and disassembly of actin filaments at the boundaries between bare and decorated filaments [1] under sub-saturating concentrations[2] Within this family the sequence homology between ADF and cofilin is 72% identical (Figure 3.1). The majority of residue differences occur in the C-terminal region. There have been reported important structural differences between ADF and cofilin that contribute to the biochemical activities of the two proteins. The activities of the ADF/cofilin family of proteins are regulated by phosphorylation of a conserved N-terminal serine residue (Ser3) and by phosphoinositide binding.[3] ADF/cofilin proteins are pH-sensitive and show a higher depolymerizing activity at pH 8 compared with pH 6.5.

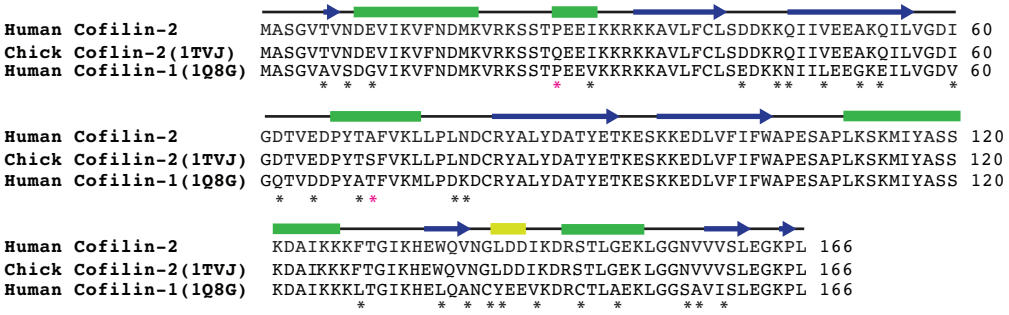

Figure 3.1: Primary sequences and secondary structure of cofilin: human cofilin-2 (secondary structure from solution NMR), chick cofilin-2 (PDB: 1TVJ) and human cofilin-1 (PDB 1Q8G). Shown in green rectangle are α-helices, blue arrows represent β-sheets, and bright green rectangle is a 3/10 α-helix. Marked with black asterisks are residues that differ between human cofilin-1 and human cofilin-2 sequence, and with red asterisks those that differ between human-cofilin-2 and chick cofilin-2 sequence.

Investigations of the structural differences of ADF and human cofilin-2 have been previously reported by X-ray crystallography and solution NMR. Work by Pope et al. reports a high resolution three-dimensional structure for human cofilin solved by solution NMR[4]. The principal structural differences between cofilin and ADF have been attributed to unique determinants in F-actin binding and G-actin binding sites between cofilin and ADF.

The binding site of cofilin and ADF proteins to F-actin requires two sites, the first site that interacts with subdomains 1 and 2 of the n actin protomer and the 1 and 3 of the adjacent n+2 actin protomer. The interaction of cofilin binding between these two actin protomers will weaken the lateral and longitudinal contacts between the subunits and therefore induce a twist change in F-actin. Residues important for F-actin binding have been identified in a wide variety of ADF/cofilins using site-directed

mutagenesis. Changes in F-actin binding of yeast cofilin when residues K96, D98, E151, K152, G155 was substituted by alanine.[5]

In this chapter, we discuss the resonance assignments of free cofilin from solution NMR. The aim of this work was to assign free cofilin residues to help aid in solid-state NMR assignments and to later analyze chemical shift perturbations between free cofilin and cofilin in complex with actin filaments.

3.2 Experiments and Methods

3.2.1 Materials

$^{15}NH_4Cl$ and U-$^{13}C_6$ glucose were purchased from Cambridge Laboratories, Inc. Common chemicals were purchased from Fisher Scientific or Sigma-Aldrich.

3.2.2 Expression and Purification of Human Cofilin-2

Expression and purification of U-^{13}C, ^{15}N- human cofilin-2 was performed by our collaborators, Drs. Elena Kudryashova and Dmitri Kudryashov's at The Ohio State University. The expression and purification was carried out as described previously[6].

3.2.3 NMR Experiments

Solution NMR spectra were acquired on a 14.1 T (^1H Larmor frequency of 600.1 MHz) Bruker AVANCE spectrometer using a triple-resonance inverse detection (TXI) probe. All spectra of U-^{13}C, ^{15}N-cofilin-2 were recorded at 298 K. Backbone and C^{β} resonance assignments of U-^{13}C,^{15}N cofilin-2 were carried out using heteronuclear 2D ^1H-^{15}N HSQC and 3D HNCACB, HNCACO, HNCA, HNCO at 298 K.

All spectra were processed with NMRpipe.[7] ^{13}C and ^{15}N chemical shifts were referenced with respect to the external standards adamantine and NH_4Cl, respectively.

3.3 Resonance Assignments

For resonance assignments of U-^{13}C,^{15}N-cofilin-2, we have recorded the following two-dimensional and three-dimensional heteronuclear spectra at 14.1T: ^{15}N-^{1}H HSQC, HNCA, HNCO, HNCACB, HNCACO. This set of spectra was collected in order to obtain site-specific resonance assignments for backbone cofilin residues. The heteronuclear ^{15}N-^{1}H HSQC spectrum of free cofilin is shown below in Figure 3.2.

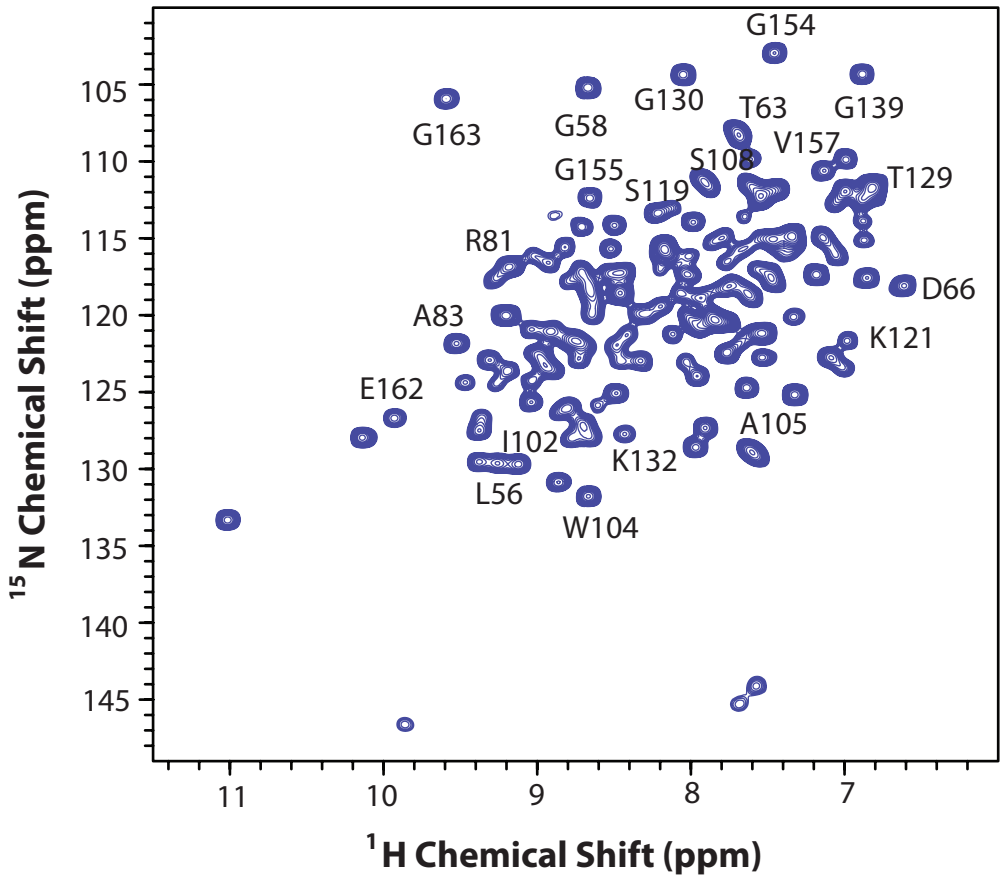

Figure 3.2: ^{15}N-^{1}H HSQC spectrum of free U-^{13}C,^{15}N-cofilin 2 at 14.1 T. Chemical shift assignments for select amino acids are labeled on the spectrum.

The backbone walk for a stretch of cofilin residues from a set of 3D experiments, HNCA, HNCO, HNCACB and HNCACO, is shown in Figure 3.3. This set of spectra allowed for the completion of backbone assignments for the free cofilin residues. Overall, we have been able to assign 80% of sidechain and backbone resonances in free cofilin (Table 3.1). Approximately 130/166 isolated peaks to be observed. By the amino acid types, Ala (9/9), Arg (5/5), His (1/1), Thr (8/8), and Trp (2/2) were completely assigned. The most problematic residues were the highly overlapped lysines, with 17/23 residues having been assigned. Residues Gly (9/13),

Leu (7/14) and Val (12/15) were also challenging due to the large number of these residue types in the sequence and the somewhat limited sensitivity of the 3D spectra due to the aged hardware on the solution 600 MHz NMR spectrometer.

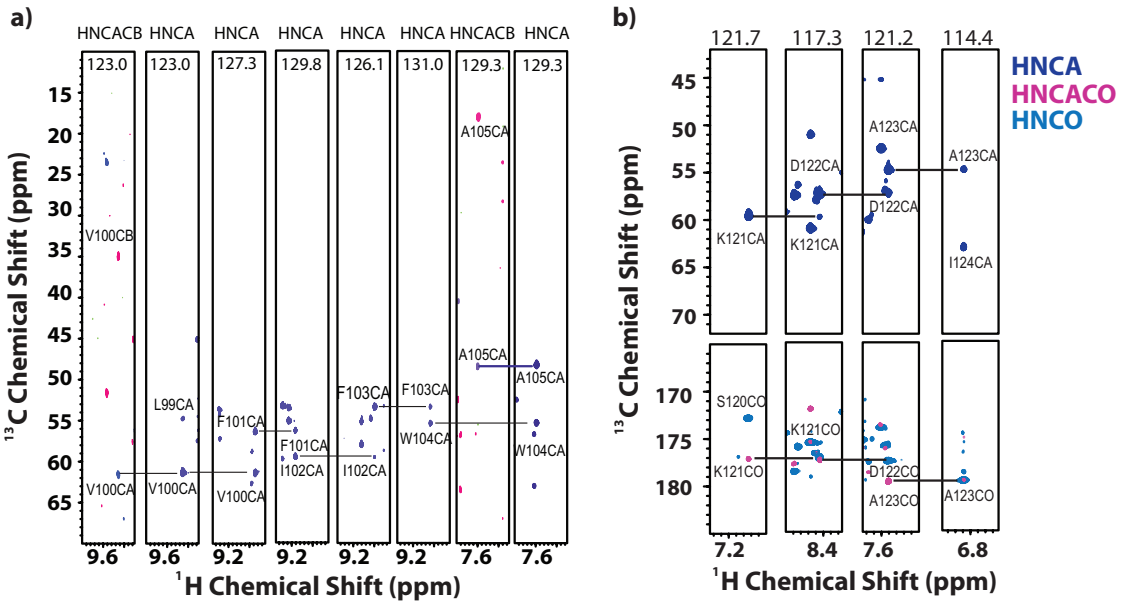

Figure 3.3: (a) HNCACB (pink) and HNCA (blue) backbone walk of cofilin-2 3D solution NMR experiments at 14.1 T for V100- A105 residues. (b) HNCACO (pink), HNCA (blue) and HNCO (light blue) backbone walk of cofilin-2 3D solution NMR experiments at 14.1 T for S120-I124.

Table 3.1: Table of chemical shifts for free U-^{13}C, ^{15}N- cofilin from solution NMR experiments at 14.1 T.

Residue Number	Type	HN Chemical Shift (ppm)	N Chemical Shift (ppm)	Cα Chemical Shift (ppm)	CO Chemical Shift (ppm)	Cβ Chemical Shift (ppm)
1	MET					
2	ALA					
3	SER			57.0	178.2	
4	GLY	8.1	104.3	47.7	174.5	
5	VAL	7.9	120.1	59.1	179.5	29.1
6	THR	7.3	120.2	57.9	177.7	
7	VAL			62.7	175.7	
8	ASN	8.0	123.0	56.0	177.9	
9	ASP	8.2	119.5	56.7	178.8	
10	GLU	8.0	119.0	58.5	179.2	
11	VAL	8.0	120.9	65.0	177.4	
12	ILE	7.7	120.7	64.3	177.7	
13	LYS	7.7	120.7	59.9	178.7	
14	VAL	8.1	118.6	66.4	178.2	31.5
15	PHE					
16	ASN					
17	ASP					
18	MET				177.4	
19	LYS	8.0	117.6	57.9	177.0	31.9
20	VAL	7.2	117.4	62.7	175.7	32.4
21	ARG	8.0	123.0	56.0	176.0	
22	LYS	8.5	123.1	56.8	176.6	33.2
23	SER	8.5	117.3	57.9	174.6	64.1
24	SER	8.6	118.9	59.5		64.4
25	THR	7.1	112.8	61.1		
26	GLN					
27	GLU					
28	GLU			60.0	175.7	
29	ILE	7.6	119.0	66.0	178.4	
30	LYS	7.1	115.5	58.0	177.3	
31	LYS					

32	ARG	8.8	121.6	57.3	176.1	
33	LYS			57.3	175.9	
34	LYS	9.5	124.5	55.1	173.3	
35	ALA	7.8	116.7	51.0	175.5	23.5
36	VAL					
37	LEU					
38	PHE					
39	CYS				172.3	
40	LEU	7.9	118.5	54.2	178.6	
41	SER	9.3	117.6	58.2	176.6	64.3
42	ASP			58.9	177.8	
43	ASP	7.8	120.8	61.9	177.2	33.3
44	LYS			61.9	174.9	
45	ARG	8.7	128.1	55.2	176.2	
46	GLN	9.0	125.7	58.0	178.3	
47	ILE					
48	ILE			62.7	175.8	
49	VAL	8.7	120.1	63.6	175.9	32.4
50	GLU			58.0	178.3	
51	GLU	9.2	120.1	59.3	176.6	
52	ALA	8.7	118.4	53.5	177.8	
53	LYS			57.9	177.3	
54	GLN	8.2	115.6	53.7	174.5	
55	ILE	8.6	119.6	59.8	175.0	
56	LEU	9.4	129.6	53.3	178.2	
57	VAL	9.2	123.7	66.8	179.5	31.2
58	GLY	8.7	105.3	46.0	173.9	
59	ASP					
60	ILE					
61	GLY				173.6	
62	ASP	8.3	120.0	54.6	175.5	47.8
63	THR	7.7	108.0	61.8	174.7	
64	VAL			58.0	177.3	
65	GLU	7.5	117.9	55.4	177.3	
66	ASP	6.6	118.2	52.4	174.6	
67	PRO			64.8	176.2	
68	TYR	8.0	119.9	63.0	177.2	
69	THR	7.8	115.0	66.3	177.5	68.7
70	SER	8.1	116.1	63.5	175.3	62.6

71	PHE	8.0	124.1	60.0	178.6	38.6
72	VAL	8.7	117.1	57.4	177.9	39.9
73	LYS	7.5	117.2	56.1	176.6	41.9
74	LEU					
75	LEU	7.8	120.3	53.2		
76	PRO					
77	LEU					
78	ASN			51.0	173.9	
79	ASP	7.3	114.8	52.8	173.1	43.9
80	CYS	7.6	115.0	57.3	173.9	29.1
81	ARG	9.0	116.3	54.1	175.7	
82	TYR	8.2	115.9	55.1	174.9	41.8
83	ALA	9.5	122.0	51.6	176.2	23.5
84	LEU	8.0	116.2	53.8	174.5	
85	TYR	8.7	122.9	57.1	173.1	
86	ASP	8.0	128.7	52.4	173.3	40.5
87	ALA	8.8	128.5	51.7	177.1	20.3
88	THR	8.4	119.9	62.1	173.2	
89	TYR	9.0	124.4	55.9	172.3	39.2
90	GLU	8.2	116.9	55.0	176.7	
91	THR	8.7	114.4	59.4	174.6	
92	LYS	8.8	117.8	59.0	176.9	
93	GLU	8.0	114.1	57.5	176.4	32.0
94	SER	7.5	112.0	58.2	172.4	66.1
95	LYS	8.3	123.0	56.9	176.0	
96	LYS	8.9	126.4	54.8	173.8	
97	GLU	7.6	117.1	54.7	176.0	32.4
98	ASP	9.0	121.0	54.5	173.6	47.8
99	LEU	8.3	120.0	54.8	176.5	47.8
100	VAL	9.3	123.0	61.4	174.8	35.0
101	PHE	8.7	127.3	56.3	173.9	
102	ILE	9.1	129.8	59.5	174.1	
103	PHE	8.8	126.1	53.4	172.5	39.3
104	TRP	8.9	131.0	55.3	171.8	
105	ALA	7.6	129.3	48.2	172.3	18.0
106	PRO					
107	GLU			58.8	177.3	
108	SER	7.7	108.6	58.2	174.6	63.1
109	ALA	7.3	125.3	50.3	174.4	18.0

110	PRO					
111	LEU	8.8	127.0	58.9	178.8	
112	LYS	8.8	115.7	59.7	179.2	
113	SER	7.1	112.8	61.1	176.1	63.3
114	LYS	8.1	121.2	60.8	179.8	
115	MET	8.5	115.7	59.1	179.4	32.7
116	ILE	7.9	120.9	64.6	179.5	38.0
117	TYR	8.9	121.2	62.1	180.9	
118	ALA	9.0	123.5	56.1	180.5	18.0
119	SER	8.2	119.0	61.2	180.5	63.2
120	SER	7.4	115.0	58.3	172.8	63.7
121	LYS	7.0	121.7	59.7	176.6	31.2
122	ASP	8.4	117.3	57.2	177.4	40.3
123	ALA	7.5	121.2	54.7	179.6	17.6
124	ILE	6.9	114.4	62.9	175.1	
125	LYS	7.7	121.9	59.4	178.9	
126	LYS	7.6	115.6	58.3	178.3	
127	LYS	7.4	115.9	56.0	175.8	32.8
128	PHE	7.6	121.4	56.9	176.1	
129	THR	7.0	111.5	66.1	178.2	
130	GLY	8.1	104.3	47.7	174.5	
131	ILE			61.5	174.5	
132	LYS	8.4	127.8	57.2	175.9	
133	HIS	7.1	116.2	55.4	173.3	34.6
134	GLU	8.9	123.7	54.1	174.7	33.2
135	TRP	9.4	127.7	53.6	173.8	33.3
136	GLN	9.3	129.8	55.2	173.5	
137	VAL	8.5	125.2	60.5	174.5	
138	ASN	9.0	122.9	52.9	174.6	34.3
139	GLY	6.9	104.3	45.1	173.4	
140	LEU					
141	ASP	8.5	114.3	60.0	174.9	
142	ASP	8.9	121.0	58.7	177.6	
143	ILE	8.5	118.4	59.2	178.2	
144	LYS	7.6	118.4	58.5	179.2	
145	ASP			55.2	175.5	
146	ARG	7.9	127.4	59.3	176.6	
147	SER			61.4	175.7	
148	THR	7.9	120.0	65.7		67.9

149	LEU			57.5	173.4	
150	GLY	9.0	122.5	45.1	178.6	
151	GLU					
152	LYS					
153	LEU				177.2	
154	GLY	7.5	103.0	45.9	174.2	
155	GLY	8.7	112.5	46.4	175.0	
156	ASN	8.8	121.9	54.5	175.0	
157	VAL	7.1	110.6	61.7	176.2	
158	VAL	7.5	122.7	63.8		
159	VAL					
160	SER					
161	LEU			54.5	176.2	47.8
162	GLU	10.0	126.9	56.1	176.7	
163	GLY	9.6	105.9	45.2	174.0	
164	LYS					
165	PRO					
166	LEU					

REFERENCES

(1) Suarez, C.; Roland, J.; Boujemaa-Paterski, R. *Curr. Biol.* **2011**, *21*, 862.

(2) Andrianantoandro, E.; Pollard, T. D. *Mol. Cell* **2006**, *24*, 13.

(3) Yang, N.; Higuchi, O.; Ohashi, K.; Nagata, K.; Wada, A.; Kangawa, K.; Nishida, E.; Mizuno, K. *Nature* **1998**, *393*, 809.

(4) Pope, B. J.; Zierler-Gould, K. M.; Kuhne, R.; Weeds, A. G.; Ball, L. J. *J. Biol. Chem.* **2004**, *279*, 4840.

(5) Lappalainen, P.; Fedorov, E. V.; Fedorov, A. A.; Almo, S. C.; Drubin, D. G. *EMBO J.* **1997**, *16*, 5520.

(6) Galkin, V. E.; Orlova, A.; Kudryashov, D. S.; Solodukhin, A.; Reisler, E.; Schroder, G. F.; Egelman, E. H. *Proc. Natl. Acad. Sci. USA* **2011**, *108*, 20568.

(7) Delaglio, F.; Grzesiek, S.; Vuister, G. W.; Zhu, G.; Pfeifer, J.; Bax, A. *J. Biomol. NMR* **1995**, *6*, 277.

Chapter 4

THREE-DIMENSIONAL STRUCTURE CHARACTERIZATION OF COFILIN-2 IN ASSEMBLY WITH F-ACTIN-ADP BY MAS NMR SPECTROSCOPY

4.1 Introduction

Actin dynamics are regulated via actin-binding proteins, such as cofilin, and via the nucleotide state of F-actin. Actin polymerization/depolymerization and filament severing have been extensively studied via X-ray fibre diffraction[1] and cryo-EM[2-7]; however, atomic-level structural information of actin-associated proteins assembled on F-actin has not been inaccessible. Magic-angle-spinning NMR studies reported here yielded atomic-resolution information on the human cofilin-2/F-actin assemblies.

In this chapter, three-dimensional structure characterization of human cofilin-2 assembled on actin filaments will be discussed.

4.2 Experiments and methods

4.2.1 Materials

$^{15}NH_4Cl$ and U-$^{13}C_6$ glucose were purchased from Cambridge Laboratories, Inc. Common chemicals were purchased from Fisher Scientific or Sigma-Aldrich.

4.2.2 Expression and purification of human cofilin/F-actin assemblies

Expression and purification of U-^{13}C, ^{15}N- cofilin-2 in complex with skeletal actin were performed by our collaborators, Drs. Elena Kudryashov and Dmitri

Kudryshov's at The Ohio State University. The expression and purification was carried out as described previously.[4]

4.2.3 Preparation of MAS NMR Samples of cofilin/F-actin assemblies

For each MAS NMR sample preparation, a solution of cofilin and F- actin in 20 mM Pipes, pH 6.8, 0.1 mM ATP, 0.2 mM $CaCl_2$, 0.4 mM EGTA, 0.1 mM TCEP, 0.1 mM PMSF, 2 mM $MgCl_2$, 25 mM KCl was centrigufuged in a TLA 120.2 rotor using a Beckman Coulter Optima MAX-TP ultracentrifuged for one hour at 90,000 rpm (RCF 352,700) at 4°C. A 10 μL aliquot was removed from the supernatant and loaded on to SDS-PAGE gel to ensure cosedimation of the cofilin/actin assembly. Cofilin/F-actin assemblies were then packed into a 1.9 mm rotor. The total amount of cofilin/actin complex sample packed into the rotor was 14 mg. Of this, the approximate amount of isotopically labeled cofilin-2 was 3 mg.

4.2.4 Characterization of cofilin/F-actin assemblies

Negatively stained TEM was used for the characterizing the morphology of cofilin/F-actin assemblies before MAS NMR experiments. Actin samples were stained with uranyl acetate (5% w/v), deposited on 400 mesh, formvar/carbon-coated copper grids, and dried. The TEM images were acquired by a Zeiss Libra 120 transmission electron microscope operating at 120 kV (Figure 4.1). The TEM images reveal that the actin morphology is intact and there is no sample degradation.

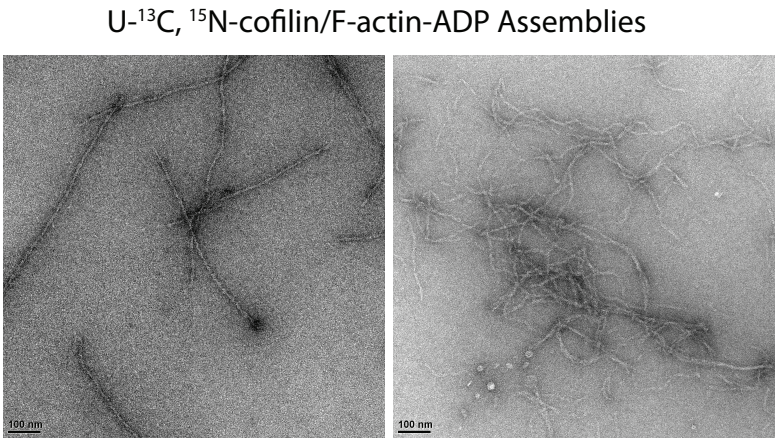

Figure 4.1: TEM images of U-^{13}C, ^{15}N-cofilin/F-actin-ADP complex before MAS NMR experiments.

4.2.5 NMR Experiments

MAS NMR spectra of U-^{13}C, ^{15}N-cofilin-2/F-actin-ADP were acquired on a 19.96 T Bruker AVIII instrument using a 1.9 mm HCN probe. The Larmor frequencies were 850.4 MHz (^{1}H), 213.8 MHz (^{13}C) and 86.2 (^{15}N). The MAS frequency was 14 kHz and controlled within ± 10 Hz by a Bruker MAS Controller. The temperature was calibrated for this probe using KBr as the temperature sensor and the actual temperature at the sample was maintained to within ±0.1°C using a Bruker temperature controller. 2D CORD, NCA, NCACX, NCOCX and 3D NCACX and NCOCX spectra were collected at 273 K.

Dipolar-based 2D and 3D NCACX and NCOCX experiments were acquired for U-^{13}C, ^{15}N-cofilin-2/F-actin-ADP complex. Non-uniform sampling (NUS) was employed for 2D and 3D NCACX and NCOCX spectra of U-^{13}C, ^{15}N-cofilin-2/F-actin-ADP complex. The exponentially weighted NUS schedules were constructed so as to yield artifact-free spectra.[8,9] The spectrum was acquired with 25% NUS using 48

complex points in t_1 and t_2 indirect dimensions, with maximum evolution times of 3.4 ms and 6.9 ms for ^{13}C and ^{15}N, respectively. The spectra were processed using the MINT reconstruction protocol.[9] The typical 90° pulse lengths were 2.75 μs, 2.95 μs for ^{13}C, and 3.3 μs for ^{15}N. The ^{1}H-^{13}C and ^{1}H-^{15}N CP employed a linear amplitude ramp for 80-100%: the ^{1}H RF field was 91 kHz; and the center of the ramp on the ^{13}C or ^{15}N was Hartmann-Hahn matched to the first spinning sideband. In 2D and 3D NCACX experiments, the RF field strengths were 64.9 kHz, 84.7 kHz and 91 kHz for ^{15}N, ^{13}C and ^{1}H channels, respectively. The DARR mixing sequence was applied to the ^{1}H channel and the DARR mixing time was 50 ms. Typical ^{1}H decoupling powers of 90-100 kHz were used during acquisition and evolution periods in all experiments.

Two-dimensional ^{13}C-^{13}C correlation experiments were performed using a CORD pulse sequence.[10] The typical 90° pulse lengths were 2.55 μs for ^{1}H and 2.3 μs for ^{13}C. The ^{1}H-^{13}C cross polarization employed a tangent amplitude ramp of 80-100%, the ^{1}H RF field was 75 kHz, and the center of the ramp of the ^{13}C Hartmann-Han matched the first spinning sideband. The RF field on the proton channel was matched to the MAS frequency (14 kHz) and one half of it (7 kHz) during the 50 ms mixing time. The typical decoupling power was 90-100 kHz during the acquisition and evolution. The spectral width was 299.75 ω_2 and 213.83 in ω_1 with the carrier frequency set to 96.2 ppm.

MAS NMR spectra of [2-^{13}C]-glucose/U-^{15}N and [1,6-^{13}C]-glucose/U-^{15}N cofilin/F-actin-ADP were collected using a 19.9 T Bruker AVIII instrument using a 1.9 mm HCN probe. The MAS frequency was 14 kHz and controlled within ± 10 Hz by a Bruker MAS controller. The temperature was calibrated for this probe using KBr

as the temperature sensor, and the actual temperature at the sample was maintained to within ±0.1°C using a Bruker temperature controller.

A 2D phase-shifted PAIN-CP[11] experiment was acquired for [2-^{13}C]-glucose/U-^{15}N and [1,6-^{13}C]-glucose/U-^{15}N cofilin/F-actin-ADP. During the PAIN-CP mixing period, RF field strengths for 1H, 15N, 13C channels were 60 kHz. The length of the PAIN-CP mixing period was 5 ms. The conditions for ^{1}H 90, ^{1}H-^{15}N cross polarization and acquisition decoupling as the same as the NCACX and NCOCX experiments.

The combined $R2_n^{\nu}$-driven (CORD) pulse sequence was employed for two-dimensional ^{13}C-^{13}C correlation experiments. The typical 90° pulse lengths were 2.55 μs for ^{1}H and 2.3 μs for ^{13}C. The ^{1}H-^{13}C cross polarization employed a tangent amplitude ramp of 80-100%, the ^{1}H RF field was 75 kHz, and the center of the ramp of the ^{13}C Hartmann-Han matched the first spinning sideband. The RF field on the proton channel was matched to the MAS frequency (14 kHz) and one half of it (7 kHz) during the 50-500 ms mixing time. The typical decoupling power was 90-100 kHz during the acquisition and evolution. The spectral width was 299.75 in ω_2 and 213.83 in ω_1 with the carrier frequency set to 96.2 ppm.

All data were processed with NMRpipe.[12] ^{13}C and ^{15}N chemical shifts were referenced with respect to the external standards adamantine and NH_4Cl, respectively.

4.3 Resonance assignments

For resonance assignments of U-^{13}C, ^{15}N-cofilin/F-actin assemblies, we have recorded the following two-dimensional and three-dimensional homo-and heteronuclear spectra at 19.9 T: NCA, CORD, NCACX, and NCOCX (Figure 4.2).

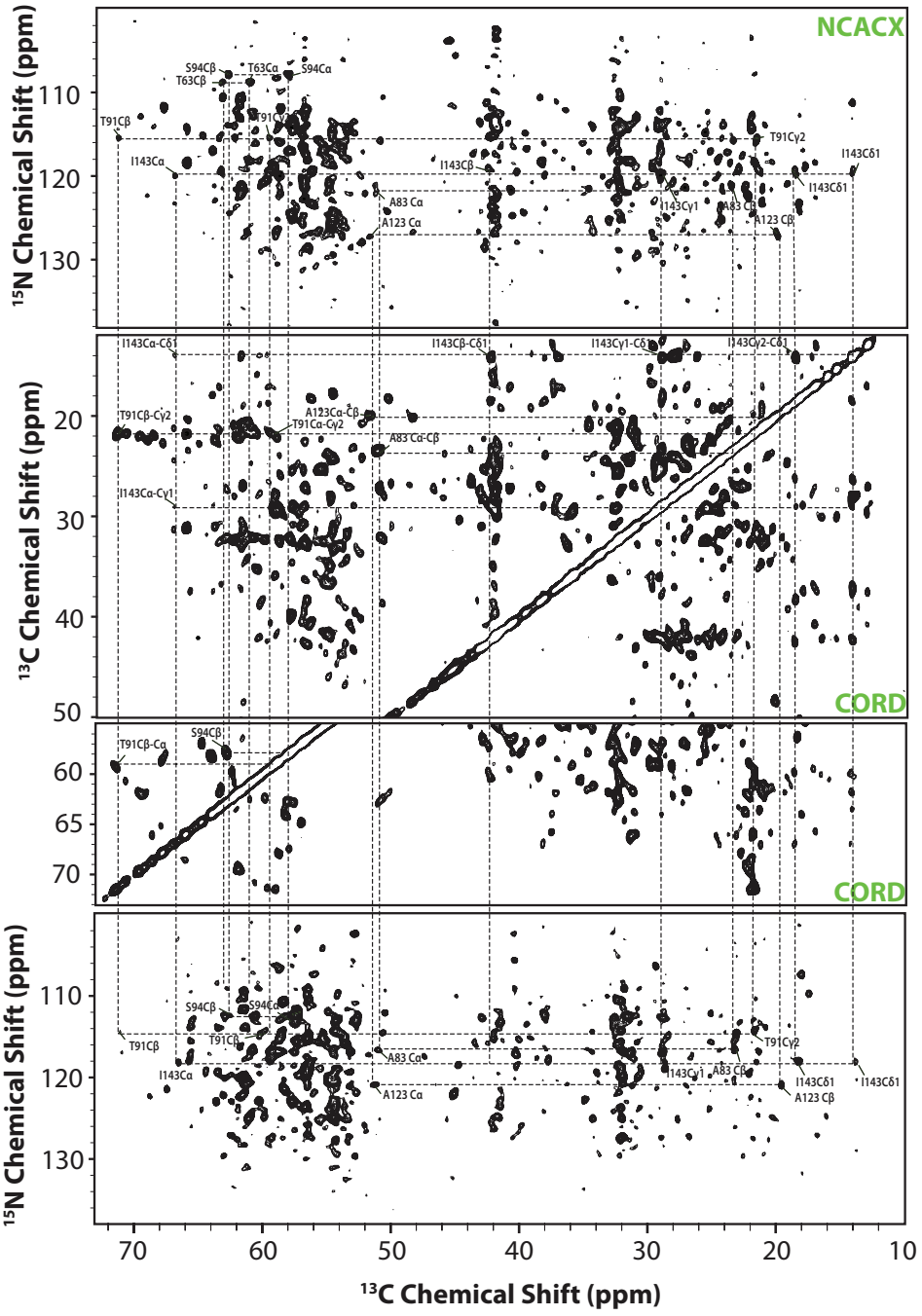

Figure 4.2: 2D and 3D MAS NMR spectra of cofilin in complex with actin, acquired at 19.9 T. (A) 2D NCACX (top), CORD (middle), and NCOCX (bottom) spectra. Selected chemical shift assignments and backbone walks are illustrated in the spectra for cofilin residues.

^{13}C-^{13}C correlation spectrum yields information regarding the amino acid type and the sidechain chemical shifts. This experiments is commonly used to establish amino acid type specific assignments. In the cofilin-2/actin assembly spectrum, unique regions for Ala, Gly, Ile, Pro, Ser, Thr, and Val were observed, as expected (Figure 4.3). With the amino acid type assignments from the ^{13}C-^{13}C CORD spectrum, nitrogen chemical shifts are next found in heteronuclear two-dimensional and three-dimensional spectra, NCA and NCACX. The heteronuclear spectra also help resolve the chemical shift degeneracy in the ^{13}C dimensions for a number of amino acid types. The three-dimensional MAS NMR NCACX spectra are shown in Figure 4.4. As illustrated in Figure 4.2 and 4.4, cofilin/actin complexes yield outstanding-resolution MAS NMR spectra.

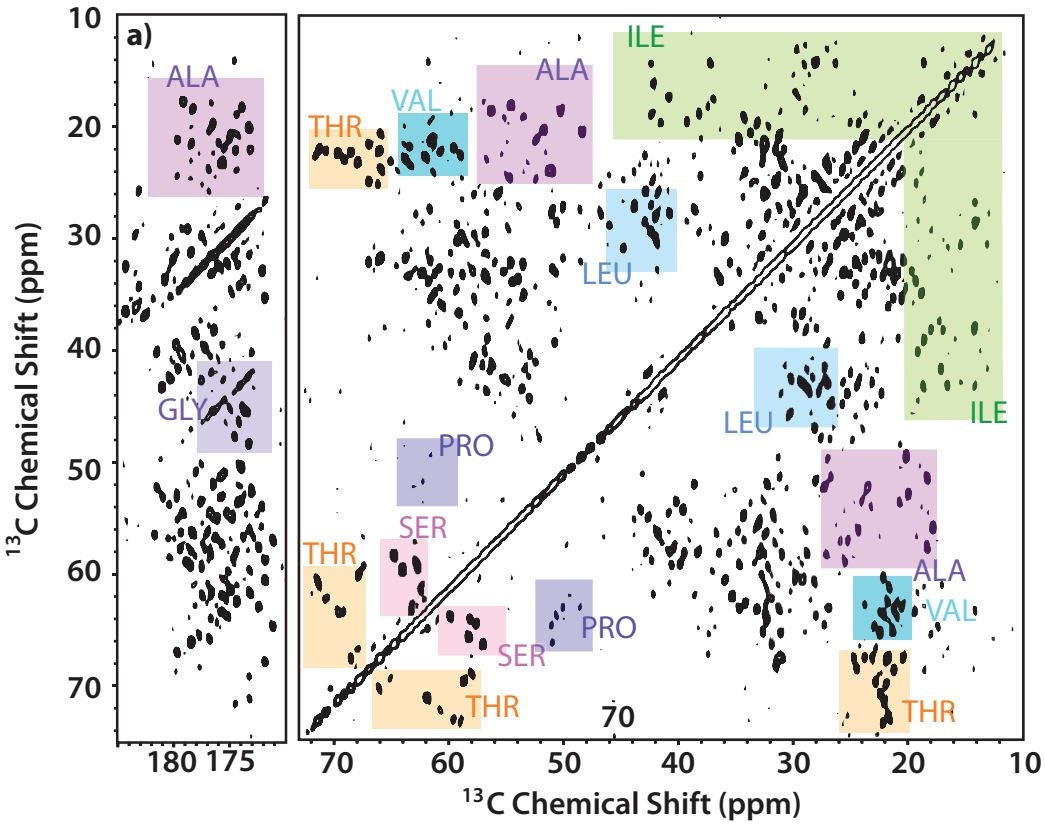

Figure 4.3: 19.9 T ^{13}C-^{13}C CORD correlation spectrum for cofilin-3/F-actin-ADP: aliphatic region (right) and carbonyl region (left). Cross-peaks corresponding to different amino acid types appear in distinct resolved regions of the spectrum and are color coded on the spectrum. Note the overall remarkable spectral resolution.

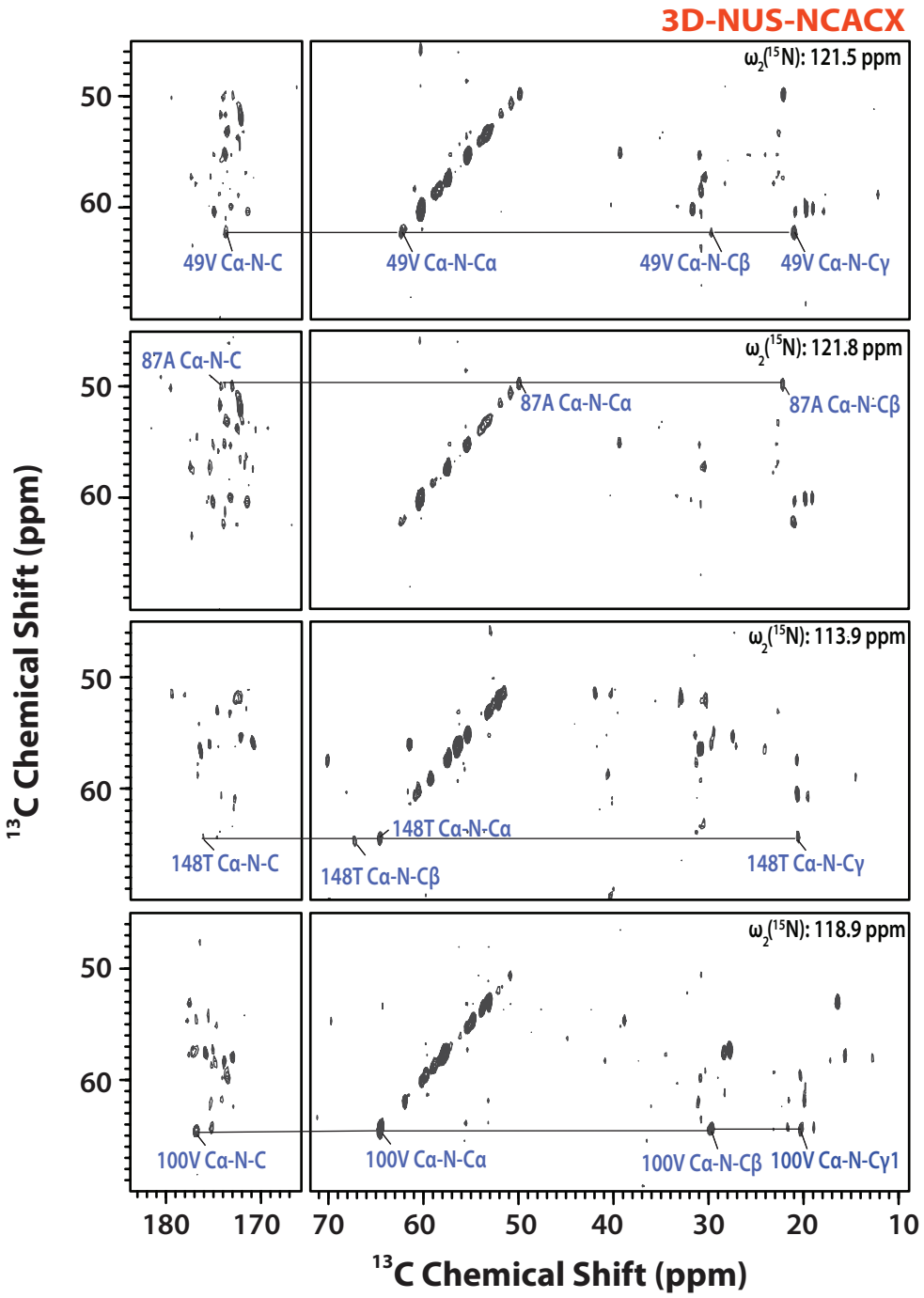

Figure 4.4: Select 2D planes of 3D NUS MAS NMR NCACX spectra of U-^{13}C,^{15}N-cofilin/F-actin-ADP complex acquired at 19.9 T. The 3D spectra were acquired with 25% NUS with 48 t_1 x t_2 complex points and the maximum evolution times are 3.4 ms and 6.9 ms for ^{13}C and ^{15}N, respectively.

3D NUS NCACX and NCOCX spectra are shown in Figure 4.4 and 4.5, respectively. The 3D experiments exhibited adequate sensitivity in sidechain carbons to assign cofilin residues. In Figure 4.5, a comparison between 2D and 3D NUS MAS NMR spectra is also shown.

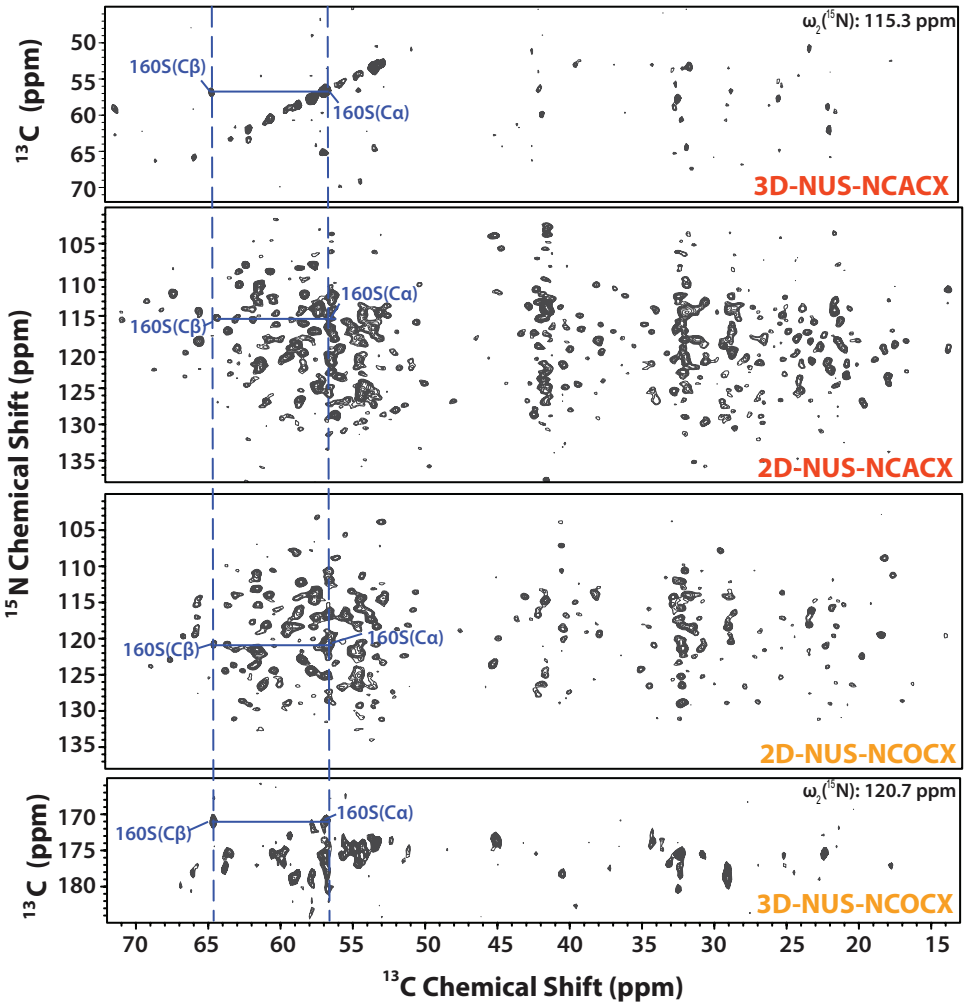

Figure 4.5: Select 2D planes of NUS MAS NMR spectra (A) 3D NCACX, (B) 2D NCACX, (C) 2D NCOCX and (D) 3D NCOCX of U-^{13}C, ^{15}N-cofilin in complex with actin acquired at 19.9 T. The 3D spectra were acquired with 25% NUS with 48 t_1 x t_2 complex points and the maximum evolution times are 3.4 ms and 6.9 ms for ^{13}C and ^{15}N, respectively.

Combining information from the 3D NCACX and NCOCX spectra with that from the CORD data set, we have assigned 70% of cofilin-2 backbone residues (Table 4.1). This includes the site-specific assignments of resonances for 111 out of 166 residues. The majority of backbone resonances are present in the spectra with the exception of the termini residues (M1, P165, L166) and several sequence stretches in loop regions spanning residues K30-K34, V72-D79, G130-Q136. Residue assignments for spin systems have been completed for each residue in cofilin for Ala (9/9), Thr (8/8), Trp (2/2), and Cys (2/2). Lys and Asp presented challenges in assignments due to their large number in the sequence and spectral overlap, resulting in partial assignments: Lys (16/23) and Asp (7/14). Correlations for the remaining residues were either missing or resided in spectral regions with limited resolution. The assignments of cofilin are summarized in Table 4.1.

A summary of resonance assignments for the cofilin primary sequence is shown in Figure 4.7. The secondary structure determined by TALOS+ from chemical shift resonance assignments for backbone residues assigned is shown in Figure 4.6.

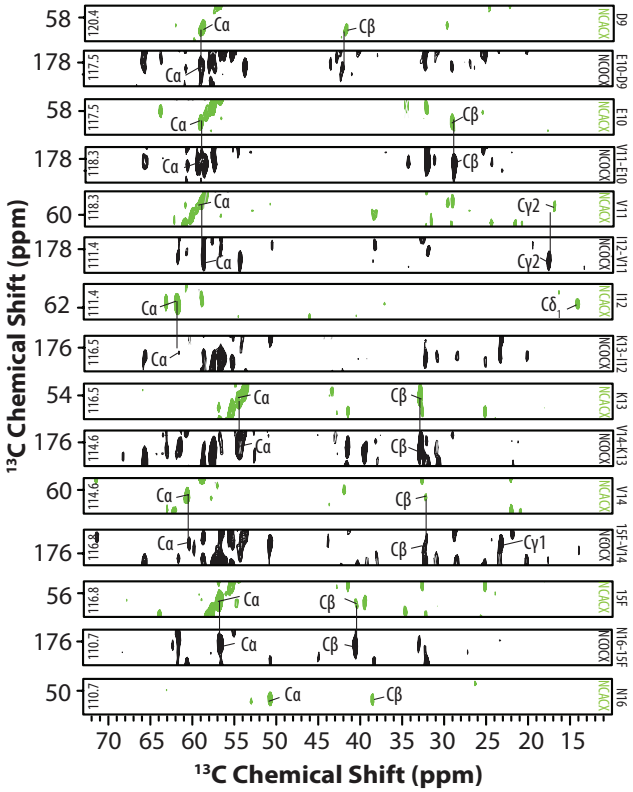

Figure 4.6: 3D NUS MAS NMR spectra for NCACX (green contours) and NCOCX (black contours) acquired at 19.9 T. Backbone walk for the stretch of residues D9-N16 obtained from 3D NCACX and NCOCX spectra.

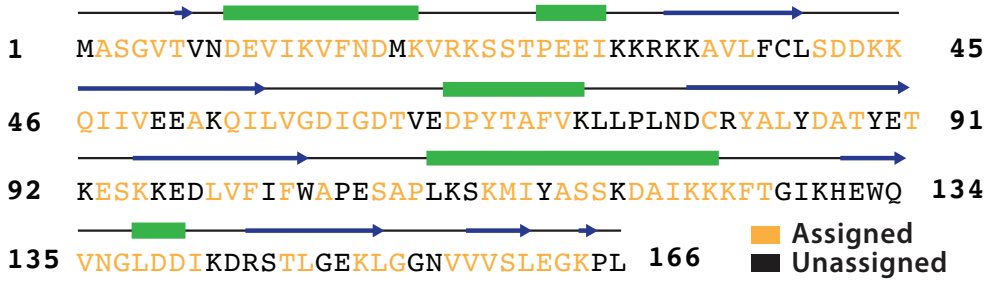

Figure 4.7: Human cofilin-2 sequence with secondary structure of cofilin-2 determined by TALOS+. Secondary structure elements, α-helix and β-strand are colored green and purple, respectively. In the primary sequence, colored in yellow and black are residues that are assigned and unassigned (not a single atom), respectively.

Table 4.1: Chemical shift assignments of nitrogen and carbon atoms in U-^{13}C,^{15}N cofilin in complex with F-actin-ADP.

	Chemical Shifts (ppm) from MAS NMR Experiments										
Residue	N	Cα	Cβ	C'	Cγ	Cγ1	Cγ2	Cδ	Cδ1	Cδ2	Cε
M1											
A2											
S3	120.8	59.8	62.5	176.0							
G4	111.5	45.3									
V5	118.2	60.8	24.7	171.3							
T6	112.5	60.8		178.4	22.0						
V7											
N8											
D9	126.5	59.0	42.0	178.4							
10E	117.9	59.4	29.2	178.4	34.3						
11V	118.1	60.5	31.9	178.1							
12I	111.1	61.8	37.2			28.7			14.2		
13K	116.5	55.0	32.8	176.4	31.0						41.6
14V	114.6	60.6	32.2	175.2		23.3					
15F	116.9	56.7	40.6	176.4							
16N	110.7	50.8	38.6	173.9	173.8						
17D	113.1	60.1	41.9								
18M											
19K	114.4	61.7	32.6	178.0	25.5						
20V	123.5	66.7	31.4	179.4		21.2	19.3				
21R	120.1	52.5	33.6	173.7	24.6			38.9			
22K	120.5	57.1	31.0	175.7							
23S	116.9	58.2	64.0	174.7							
24S	114.0	57.7	62.9	174.3							
25T	114.5	59.0	71.5				22.0				
26Q	116.6	54.0	33.0	172.0	36.4			175.6			
27E	117.2	57.8		174.2	34.7			178.3			
28E	113.6	57.5	28.5	172.4	31.1						
29I	116.9	64.0	37.4	177.4			17.8				
30K											
31K											
32R											
33K											
34K											

35A	115.7	50.9	23.5	175.4							
36V	118.4	65.9	31.3	176.7		23.6	20.4				
37L	117.1	55.5	43.0		25.3				22.4		
38F											
39C		56.7	33.5	180.4							
40L	119.7	58.9	42.0	178.4	29.2				24.5	23.5	
41S	121.4	56.5	61.6	174.6							
42D	118.2	58.7	32.3	178.4							
43D	118.0	58.6	36.9	180.2							
44K	123.4	56.7		178.0	21.8			24.4			38.2
45R	119.4	56.2		173.0				40.5			
46Q	129.5	54.5	30.8	174.5							
47I	129.1	60.4	38.9	173.3		29.8	16.2				
48I	126.7	61.3	34.3	174.0		23.9	19				
49V	121.5	63.6	31.1	175.0		22.4	22.5				
50E											
51E											
52A	115.7	55.8	19.4								
53K											
54Q	114.2	56.9	29.1	175.4							
55I	114.2	62.2	34.4	174.3			21				
56L	126.5	53.8	43.2	175.5	24.1						
57V	123.0		32.5	177.1		25.6					
58G		45.8									
59D	114.7	53.2	43.3	173.9							
60I	120.9	61.6	39.3	176.5		32.8	19.3		13.8		
61G	103.8	45.2		173.3							
62S	126.6	56.0	40.9	178.1							
63T	108.8	60.9	63.3								
64V											
65E		57.1	32.2	177.0	38.0						
66D	116.7	56.9	39.6	176.7							
67P	136.0	63.0	50.7	175.2	27.3						
68Y	112.9	62.0	69.6	175.7	21.9						
69T	111.8	58.6	68.0	171.7							
70S	123.7	59.9	42.3	175.3							
71F	121.3	63.8	32.1	175.8	21.0						
72V	116.1	58.6	32.2	177.1				27.8			42.4
73K											

74L											
75L											
76P											
77L											
78N											
79D											
80C	114.2	54.7	32.2	175.1							
81R											
82Y	116.8	54.7	41.8	175.0							
83A	121.2	51.2	23.6	173.9							
84L	114.0	53.1	41.6	177.9							
85Y											
86D		54.1		172.3							
87A	121.4	51.3	23.6	175.5							
88T	117.7	65.4	68.0				22.8				
89Y											
90E											
91T	115.6	59.6	71.2	174.8			21.8				
92K											
93E	118.9	59.2	29.5	177.0	36.0						
94S	107.8	57.9	67.7								
95K	114.1	56.7		173.5				29.0			42.1
96K											
97E											
98D											
99L	121.6	61.3	34.8		21.1						
100V	118.7	65.9	31.0	178.1		21.7					
101F	130.9	52.9	39.6	173.6							
102I											
103F	128.6	56.6	42.8								
104W											
105A	126.7	48.3	20.2	177.7							
106P				122.4							
107E											
108S		57.9	62.6	174.2							
109A	124.4	50.4	18.3	173.9							
110P	135.7		31.3		26.8			50.2			
111L											
112K											

113S											
114K	118.2	61.6	38.4	177.2	27.0			26.8			
115M	112.4	58.6	32.1	176.4							
116I	112.2	57.6	29.1			25.4					
117Y											
118A	123.3	56.3	18.3	178.2							
119S	109.7	58.4	64.1	176.5							
120S	110.7	61.5	63.2								
121K											
122D	127.2	52.3	40.1	172.8							
123A	127.5	51.5	19.9	176.3							
124I	122.9	65.7	37.6	177.4			17.1		13.1		
125K	120.7	56.8	32.4								
126K	120.9	56.9	32.5	175.4							
127K	121.2	59.1	29.7	175.6	24.4			28.3			
128F	112.4	56.6	32.8	176.1							
129T	112.6	60.8	62.4	175.7			21.9				
130G											
131I											
132K											
133H											
134E											
135W											
136Q											
137V	118.4	61.1	32.4	175.0		21.8					
138N	114.2	53.3	34.4	173.9							
139G	103.8	45.6		176.3							
140L	123.7	57.0	42.4	172.8							
121D	126.2	54.7	41.7	175.9							
142D	124.9	57.9	40.6	178.2							
143I	119.5	59.7	38.5	177.7		26.4	18.9				
144K											
145D											
146R											
147S											
148T	114.1	66.0	68.6	177.7			22				
149L	126.3	60.3	42.0	174.9	32.2						
150G											
151E											

152K		62.6	32.4	176.0				27.4			41.9
153L	117.6	56.7	43.8	178.2	26.9					23.2	
154G	103.9			47.8							
155G											
156N											
157V	119.2	63.2	32.5	175.4		22.5					
158V	119.4	63.5	32.5	175.2		22.3					
159V	121.3	61.5	33.1	176.4		21.3					
160S	115.3	56.9	64.7	171.1							
161L	121.1	56.7	40.9	175.9	27.2						
162E	126.7	55.7	25.9	176.5	34.2						
163G	105.6	45.2		173.9							
164K	120.7	59.8	32.4								
165P											
166L											

4.4 Distance restraints

To record ^{13}C-^{13}C distance restraints for structure determination, $R2_1^1$ experiments were performed with the mixing times of 50 ms, 200 ms and 500 ms, on [2-^{13}C]-glucose/U-^{15}N and [1,6-^{13}C]-glucose/^{15}N-cofilin-2/F-actin at 273 K. We have used the assigned chemical shifts for the analysis of the various $R2_1^1$ spectra. For the spectra acquired with the mixing time of 50 ms, the assignments were trivial as mostly one-bond correlations are present. In the 200 ms and 500 ms spectra, numerous cross peaks arising from sequential and long-range correlations were observed (Figure 4.8).

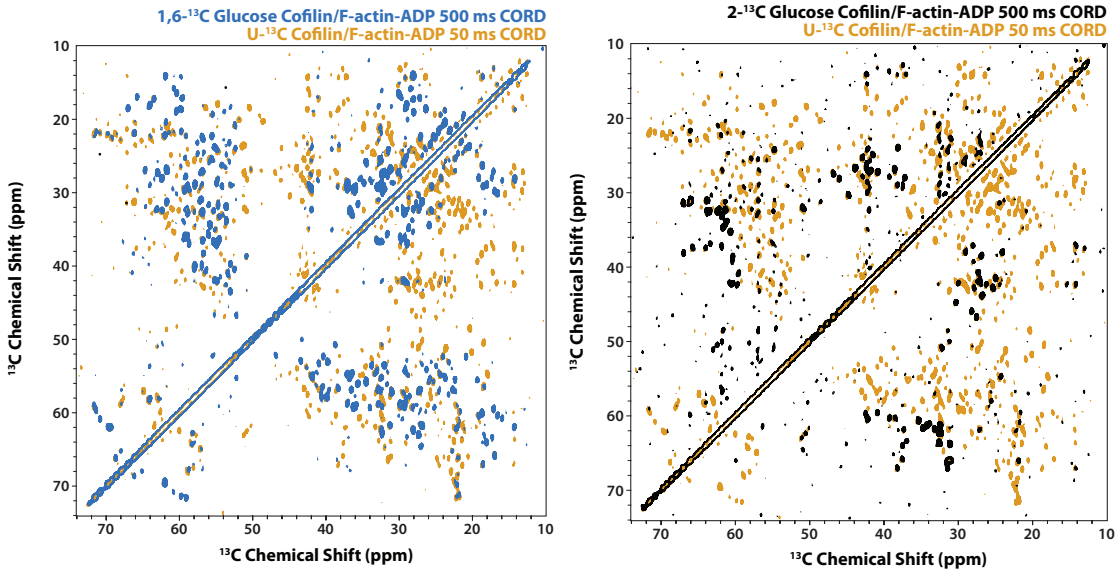

Figure 4.8: Left: Overlay of 19.96 T ^{13}C-^{13}C correlation 2D CORD spectra for U-^{13}C,^{15}N-cofilin-2/F-actin-ADP (yellow) and [1,6-^{13}C]-glucose-cofilin-2/F-actin-ADP (blue) acquired with the mixing time of 500 ms. Right: Overlay of 19.96 T ^{13}C-^{13}C-correlation 2D CORD spectra for U-^{13}C, ^{15}N-cofilin/F-actin-ADP (yellow) and [2-^{13}C]-glucose-cofilin/F-actin-ADP (black) acquired with the mixing time of 500 ms.

In Figure 4.8, it is illustrated that additional peaks in the aliphatic regions of the ^{13}C-^{13}C correlation spectrum are observed. An expansion of the aliphatic region is shown in Figure 4.9 with additional peaks observed at long mixing time shown in the gray box. These peaks arise from long-range correlations in the [2-^{13}C]-glucose/U-^{15}N/F-actin-ADP complex. The increase in the number of peaks from long-range distances adds an additional level of complexity and introduces potential ambiguity in the inter-residue assignments.

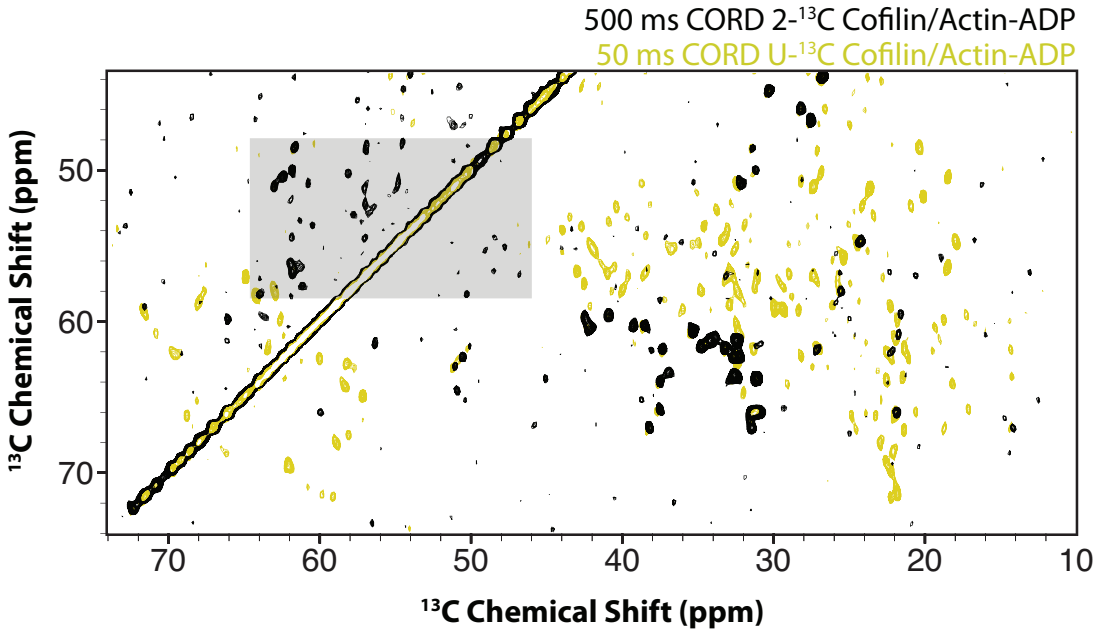

Figure 4.9: Expansion of 19.96 T 2D ^{13}C-^{13}C CORD correlation spectrum acquired with the 50 ms CORD mixing time for U-^{13}C, ^{15}N-cofilin/F-actin-ADP (yellow) and with the 500 ms CORD mixing time for [2-^{13}C]-glucose-cofilin/F-actin-ADP (black).

To extract ^{15}N-^{13}C distance restraints, a 2D phase-shifted PAIN-CP experiment was acquired for [2-^{13}C]-glucose/U-^{15}N- and [1,6-^{13}C]-glucose/^{15}N-cofilin/F-actin at 273 K (Figure 4.10). The PAIN-CP is overlaid on the NCACX spectra of U-^{13}C/^{15}N-cofilin/F-actin-ADP. The boxes represent the presence of new peaks that come from long-range correlations between ^{13}C-^{15}N resonances that are observed in the cofilin structure in the PAIN-CP experiment. From this spectra, twelve new correlations can be observed and will be used as unambiguous long-range distance restraints in the structure determination.

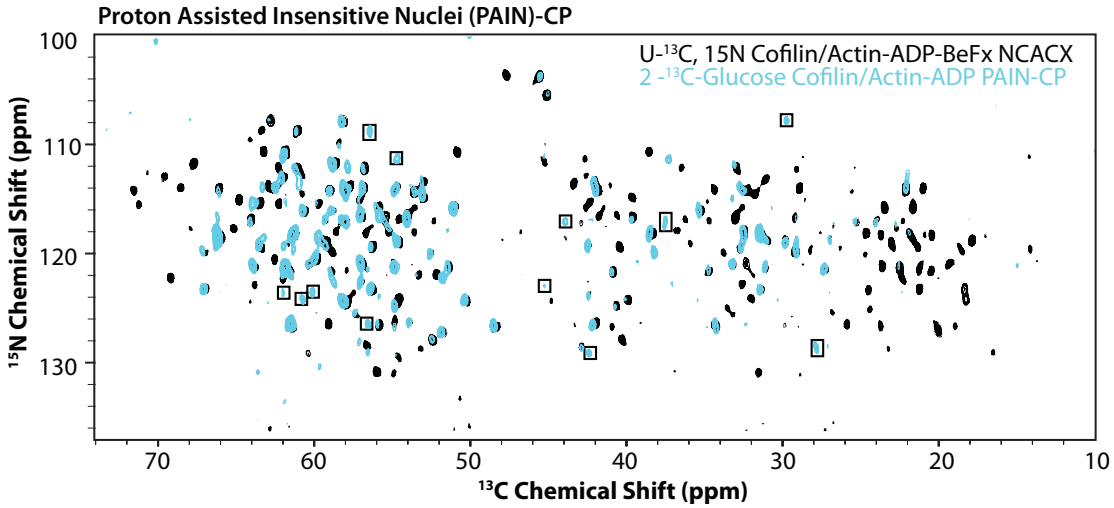

Figure 4.10: Overlay of PAIN-CP spectrum of [2-^{13}C]-glucose-cofilin/F-actin-ADP (blue) and 2D NCACX spectrum of U-^{13}C, ^{15}N-cofilin/F-actin-ADP (black) acquired at 19.96 T. Boxes represent peaks present only in PAIN-CP spectrum.

4.5 Conclusions and Future Outlook

In this work, we presented atomic-level investigation of human cofilin bound to actin filaments by MAS NMR. The outstanding spectral resolution has enabled us to gain structural information of cofilin assembled at the interface of actin filaments. To date, 70% of backbone resonance assignments of human cofilin in complex with actin have been completed by us. Distance restraints from sparsely labeled samples of cofilin in complex with actin are currently being assigned and will be used in the structure calculation. This work is ongoing and will provide the first high-resolution structure of human cofilin assembled on actin filaments.

Broadly, MAS NMR approach reported herein yields atomic-level structural information and is applicable to the analysis of actin-binding proteins assembled on filamentous actin that otherwise are not amenable to atomic-resolution studies through other current techniques.

REFERENCES

(1) Oda, T.; Makino, K.; Yamashita, I.; Namba, K.; Maeda, Y. *Biophys. J.* **2001**, *80*, 841.

(2) Fujii, T.; Iwane, A. H.; Yanagida, T.; Namba, K. *Nature* **2010**, *467*, 724.

(3) Aihara, T.; Oda, T. *Biochem. Biophys. Res. Commun.* **2013**, *435*, 229.

(4) Galkin, V. E.; Orlova, A.; Kudryashov, D. S.; Solodukhin, A.; Reisler, E.; Schroder, G. F.; Egelman, E. H. *Proc. Natl. Acad. Sci. USA* **2011**, *108*, 20568.

(5) Kudryashov, D. S.; Galkin, V. E.; Orlova, A.; Phan, M.; Egelman, E. H.; Reisler, E. *J. Mol. Biol.* **2006**, *358*, 785.

(6) Muhlrad, A.; Kudryashov, D.; Michael Peyser, Y.; Bobkov, A. A.; Almo, S. C.; Reisler, E. *J. Mol. Biol.* **2004**, *342*, 1559.

(7) McGough, A.; Chiu, W. *J. Mol. Biol.* **1999**, *291*, 513.

(8) Suiter, C. L.; Paramasivam, S.; Hou, G.; Sun, S.; Rice, D.; Hoch, J. C.; Rovnyak, D.; Polenova, T. *J. Biomol. NMR* **2014**, *59*, 57.

(9) Paramasivam, S.; Suiter, C. L.; Hou, G.; Sun, S.; Palmer, M.; Hoch, J. C.; Rovnyak, D.; Polenova, T. *J. Phys. Chem. B* **2012**, *116*, 7416.

(10) Hou, G.; Yan, S.; Trebosc, J.; Amoureux, J. P.; Polenova, T. *J. Magn. Reson.* **2013**, *232*, 18.

(11) Lewandowski, J. R.; De Paepe, G.; Griffin, R. G. *J. Am. Chem. Soc.* **2007**, *129*, 728.

(12) Delaglio, F.; Grzesiek, S.; Vuister, G. W.; Zhu, G.; Pfeifer, J.; Bax, A. *J. Biomol. NMR* **1995**, *6*, 277.

Chapter 5

STRUCTURAL STUDIES OF BINDING INTERFACE OF COFILIN IN ASSMBLY WITH F-ACTIN IN TWO NUCLEOTIDE STATES

5.1 Introduction

5.1.1 Cofilin/F-actin Interface

Recently, cryo-EM was used to probe cofilin/actin interactions by investigating the structural differences between F-actin and cofilin-decorated F-actin.[1] The cofilin interactions were divided into two regions: the upper site, which was previously determined to be the G-actin binding site and the lower site, known as the F-actin binding site. Actin residues 143-147 and 343-346 interact with cofilin residues 112-119 located on the top of α4-hleix. The C-terminal residues of actin (349-354) form contacts with cofilin N-terminus and loop 41-46. The actin binding region of cofilin formed by the N-terminus residues (1-5) have been reported to not necessarily be required for the binding of cofilin to the filament but may induce structural perturbations in the filament that in turn are critical in the cell. This finding is also consistent with the significant role that cofilin's N-terminus played in the activity of cofilin in the critical phosphorylation of Ser3 that regulates cofilin activity.

Additional F-actin binding sites have been observed by cryo-EM. The first contact was found between the small loop of cofilin (154-158) interacting with actin residues 242-243 located in the subdomain 4 of actin protomer. The second site was found between cofilin residues 94-98 forming extensive contacts with residues 21-28

and 90-96 in subdomain 1 of actin. Cofilin residues 19-21 also interact with actin residues 90-96 of actin.

On the basis of the extensive contacts found by this study, the investigators concluded that cofilin binding introduces a conformational change in the actin protomers and induces a helical twist of the filament. It has been previously reported that a cofilin-induced change results in a 5° change in the helical twist of F-actin between the n and n+1 actin protomers.[2] This cofilin-induced change causes a 10° rotation of protomer n and n+2 in the actin filament. This rotation in turn causes the filament to change the twist and cofilin to no longer preserve its contacts with two actin protomers due to the steric clash observed. The α1- and α4-helices of cofilin undergo a steric clash with actin subdomains 1 and 2, respectively. These clashes cause a rotation of the outer domain of actin and weaken the longitudinal contacts of the interface of SD1 and SD2 of adjacent actin protomers (Figure 5.1). It has been previously reported that the polymerization of G-actin to F-actin causes a flattening of the actin monomer and the outer domain of actin rotates approximately 20°. The binding of cofilin to actin filaments was found to rotate the outer domain 30° from its flattened position toward the opposite helical strand. This cofilin-induced change alters the longitudinal contacts between actin protomers upon cofilin binding. Further understanding of cofilin-actin interactions and the molecular mechanism of cofilin-based actin remodeling requires atomic level structural information about these assemblies.

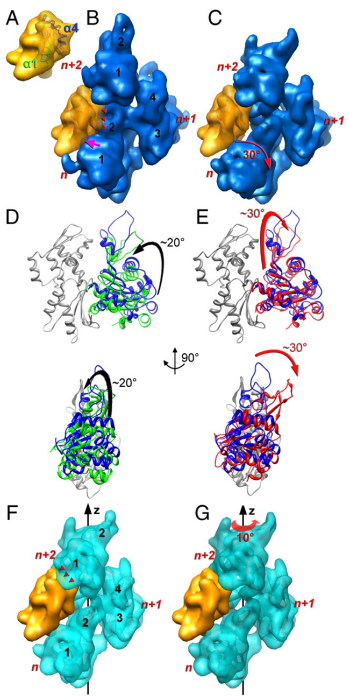

Figure 5.1: Cofilin alters the conformation of actin protomers and the helical twist of the actin filament. (a) Cofilin interacts on the surface of the actin filament (b), the α1-helix (green) of cofilin clashes with the SD1 of actin. The steric clash is indicated by the magenta arrow. A separate steric clash is observed in α4-helix (blue) and is indicated by the red arrowheads. (c) The outer domain rotates approximately 30° away from cofilin to resolve the steric clash. (d) The inner domain of actin composed of SD3 and SD4 is shown in gray and the outer domain is colored. Rotation of the outer domain from G-actin conformation (green ribbons) to F-actin conformation (blue ribbons) by approximately 20° (black arrow) flattens the molecule. (e) Upon cofilin binding the outer domain of actin rotates from the F-actin conformation (blue ribbons by approximately 30° (red arrow) toward the opposite helical strand. (f) When cofilin-deformed actin protomers (e) are arranged into a helical filament having the normal symmetry (f), the α4-helix of cofilin clashes with the lower portion of SD1 of actin (red arrowheads) (g) The clash shown in F can be resolved by the rotation of protomer n+2 by 10° around the helical axis (red arrow). Permission for reuse in this dissertation is granted by Proc. Natl. Acad. Sci., copyright 2011.[2]

Despite extensive biochemical and biophysical studies into cofilin interacting with actin filaments, the structure and binding interface between cofilin and actin filaments remains unknown. In this chapter, we report atomic-level investigation of the interface of human cofilin-2 bound to actin filaments.

5.1.2 Regulation of Actin Processes

As discussed previously in Chapter 1, monomeric actin is composed of two major domains larger (inner) and small (outer) domains. The small domains are further subdivided into subdomains 1/2, and 3/4. Actin monomers have a nucleotide-binding cleft positioned deep inside the cleft of SD2 and SD4 domains. The nucleotide is inserted between two phosphate binding loops (P1 and P2 loops) (Figure 1.3). The nucleotide binding cleft (NBC) is separated by a hinge region into a less deep cleft known as the hydrophobic cleft. This hydrophobic cleft is composed of hydrophobic amino acids and known to be a primary binding site for many actin-binding proteins.[3] The SD2 of the actin monomer is the smallest and most flexible domain and consists of the DNase I binding loop (D-loop). This loop has been reported to adopt an α-helix, β-turn or various loop conformations but is disordered in most X-ray structures of actin published to date. The N- and C-terminus are located on opposite faces of in the SD1. All structural elements of monomeric actin are influenced by the nucleotide state of actin in the filament. These elements act as sensory regions for the binding of many ABPs. The ability for ABPs to recognize the nucleotide sensing regions, such as the clefts and loops, of the actin monomers will play a very important role in the possibility for ABPs to recognize the ATP and ADP states of actin filaments.

Under physiological conditions G-actin and F-actin are in dynamic equilibrium. Upon polymerization ATP is hydrolyzed to ADP and Pi. As the ATP is hydrolyzed along the actin filament, the release of the inorganic phosphate is about two order of magnitude slower than the hydrolysis. This causes the filament to be composed of three different nucleotide states and the majority of actin protomers to exist in the ADP-Pi nucleotide state. The ADP-Pi and ATP states of actin filaments have been reported to be more structurally stable than ADP actin.[4] The release of the inorganic phosphate results in intra-and intermolecular conformational rearrangements in the filament. This causes the filament to be less stable and more flexible than ADP-actin filaments.[5]

Within the cell, treadmilling is regulated by actin-binding proteins, such as cofilin. These actin-binding proteins preferentially recognize one of the nucleotide-related conformational states of actin. It has been reported that the primary role of ATP hydrolysis in actin filaments is to create a nucleotide-related clock to create age-dependent conformational changes that can be recognized by ABPs.

In recent efforts, the nucleotide-dependent severing of actin filaments by cofilin were investigated by biochemical methods and electron microscopy. While impressive work from cryo-EM studies[1] allowed for a broader mechanistic understanding of how cofilin assists in the severing of actin filaments, this work reports, for the first time, atomic-level structural analysis of the interface of cofilin/actin complexes in two nucleotide states of actin, actin-ADP and actin-ADP-BeFx (a mimic state of ADP-Pi). Two MAS NMR approaches were used to determine the intermolecular interface of cofilin binding to actin: i) chemical shift perturbation analysis between two nucleotide states of actin (actin-ADP and actin-ADP-BeFx) and

ii) intermolecular dipolar contacts between cofilin and actin filaments determined by REDOR-filter-based experiments.

5.1.3 Determination of Intermolecular Interfaces with MAS NMR Methods

In MAS NMR, chemical shift perturbations are used to determine site-specific interactions arising due to the binding of a biomolecule to its binding partner (i.e. cofilin binding to actin filaments). This approach allows for direct observation of residues that are interacting with their binding partner and in turn experiencing a change in chemical environment. Although this approach allows for perturbations in site-specific residues to be observed, chemical shift perturbations can also be attributed to other environmental effects (i.e. solvent interactions) and allosteric effects. The second method to determine an intermolecular interface is using differentially isotopically enriched samples. In this method, one biomolecule is isotopically labeled with a certain set of isotopes (e.g. ^{13}C) and its binding partner with a different set of isotopes. (e.g. ^{15}N).[6,7] To use this method, the incorporation of isotopic labels into actin filaments needs to be implemented. To date, no protocol exists for isotopic labeling of actin. In order to circumvent this issue, we employed a recent approach developed by our laboratory, where double REDOR (dREDOR) filtered experiments are implemented to directly detect the intermolecular interface of isotopically bound cofilin assembled with natural abundance actin filaments.

In this approach, simultaneous ^{1}H-^{13}C/^{1}H-^{15}N REDOR filters dephase all cofilin protons that are directly bonded to either ^{13}C or ^{15}N atoms (i.e. ^{1}H belonging to the U-^{13}C, ^{15}N-cofilin), as shown in Figure 5.2. The remaining protons belonging to the unlabeled actin are then used to transfer the magnetization to cofilin through ^{1}H-^{15}N or ^{1}H-^{13}C cross polarization across the intermolecular interface, followed by a

HETCOR or CORD mixing (Figure 5.3). This resulting spectrum contains specific information about the residues forming intermolecular interfaces.

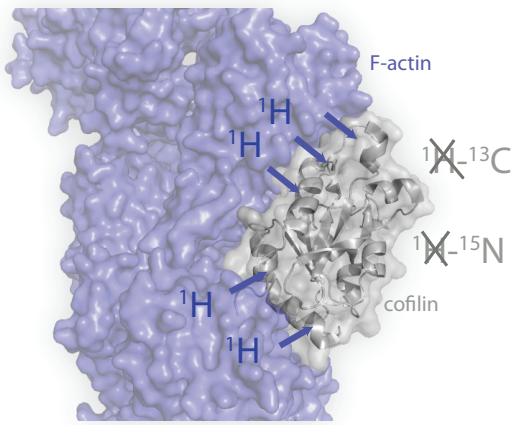

Figure 5.2: The intermolecular interface of cofilin (gray) assembled on actin filaments (purple) reconstructed from cryo-EM structure PDB 3J0S. The transfer of magnetization to cofilin ^{1}H-^{15}H or ^{1}H-^{13}C cross polarization across the intermolecular interface from actin is shown on the structure.

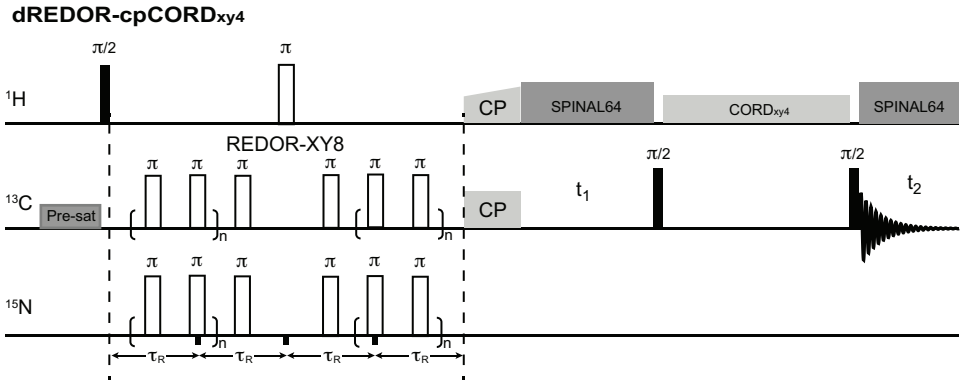

Figure 5.3: 2D ^{13}C-^{13}C correlation pulse sequence for dREDOR-CORD. ^{1}H-^{13}C/^{1}H-^{15}N REDOR dephasing periods of 714.3 μs was used to eliminate signals from 1H directly bonded to ^{13}C and ^{15}N (all the protons in cofilin). A pre-saturation π/2-pulse was applied on the ^{13}C channel before the proton excitation to remove remnant signals from the previous scan.

5.2 Experiments and Methods

5.2.1 Materials

$^{15}NH_4Cl$ and U-$^{13}C_6$ glucose were purchased from Cambridge Laboratories, Inc. Common chemicals were purchased from Fisher Scientific or Sigma-Aldrich.

5.2.2 Expression and purification of cofilin and F-actin assemblies

Expression and purification of U-^{13}C, ^{15}N- cofilin in complex was prepared by our collaborator Dr. Elena Kudryashov from the laboratory of Dr. Dmitri Kudryshov's at The Ohio State University. The expression and purification was carried out as described previously. [1]

5.2.3 NMR Experiments

MAS NMR spectra of U-^{13}C/^{15}N cofilin/F-actin-ADP and U-^{13}C/^{15}N cofilin/F-actin-ADP-BeFx were collected using a 19.96 T Bruker AVIII instrument using a 1.9 mm HCN probe. The MAS frequency was 14 kHz and controlled within ± 10 Hz by a Bruker MAS Controller. The temperature was calibrated for this probe using KBr as the temperature sensor and the actual temperature at the sample was maintained to within ±0.1°C using a Bruker temperature controller.

Dipolar-based 2D NCA and NCACX experiments were acquired for U-^{13}C, ^{15}N-cofilin-2/F-actin-ADP-BeFx complex. Two-dimensional ^{13}C-^{13}C correlation experiments were performed using a CORD pulse sequence. The typical 90° pulse lengths were 2.55 μs for ^{1}H and 2.3 μs for ^{13}C. The ^{1}H-^{13}C cross polarization employed a tangent amplitude ramp of 80-100%, the ^{1}H RF field was 75 kHz, and the center of the ramp of the ^{13}C Hartmann-Han matched the first spinning sideband. The RF field on the proton channel was matched to the MAS frequency (14 kHz) and one

half of it (7 kHz) during the 50 ms mixing time. The typical decoupling power was 90-100 kHz during the acquisition and evolution. The spectral width was 299.75 ω_2 and 213.83 in ω_1 with the carrier frequency set to 96.2 ppm.

2D REDOR-CORD spectra of U-^{13}C/^{15}N cofilin/F-actin-ADP were collected using double-REDOR filtered experiments employed simultaneous ^{1}H-^{13}C/^{1}H-^{15}N REDOR dephasing periods of 714 μs, to eliminate signals from ^{1}H (all protons in cofilin-2) directly bonding to ^{13}C and ^{15}N. All cross-polarization (^{1}H-^{13}C) and CORD transfers were performed using the parameters above for the CORD experiments. The experiments were performed using U-^{13}C, ^{15}N-cofilin-2 bound to actin-ADP. dREDOR-CORD spectra used 5 ms CP contact time and 50 ms of ^{13}C-^{13}C mixing time.

2D REDOR-CORD spectra of U-^{13}C/^{15}N cofilin/F-actin-ADP-BeFx were collected using double-REDOR filtered experiments employed simultaneous ^{1}H-^{13}C/^{1}H-^{15}N REDOR dephasing periods of 714 μs, to eliminate signals from ^{1}H (all protons in cofilin-2) directly bonding to ^{13}C and ^{15}N. All cross-polarization (^{1}H-^{13}C) and CORD transfers were performed using the parameters above for the CORD experiments. The experiments were performed using U-^{13}C, ^{15}N-cofilin-2 bound to actin-ADP. dREDOR-CORD spectra used 5 ms CP contact time and 50 ms of ^{13}C-^{13}C mixing time.

5.3 MAS NMR of Cofilin/F-Actin Complex: Intermolecular Interface and Allosteric Perturbations

5.3.1 Chemical Shift Perturbations

As discussed in Chapters 2 and 3, chemical shift interaction is a sensitive reporter of local environments within proteins. Chemical shifts in this work were used to probe conformational changes that occur upon cofilin binding to actin filaments.

To probe conformational changes in cofilin upon binding to F-actin-ADP, we have analyzed chemical shift perturbations in free cofilin in solution vs. its complex with F-actin-ADP. Since atomic-resolution structure of human cofilin-2 is not yet available, all residues identified in the present study were mapped onto the structure of homologous human cofilin-1 (PDB 1Q8G)[8] and compared with the cryo-EM reconstruction of cofilin/F-actin complex.[1] Most residues exhibit relatively small but non-trivial chemical shift perturbations indicating that the cofilin's conformation is perturbed considerably upon binding to F-actin (Figure 5.4). This finding indicates that previous assumptions that cofilin binds to F-actin as a rigid body are incorrect. Remarkably, very large chemical shift perturbations (> 2ppm) were observed for over 27% of all residues, particularly at the N-terminus (residues S3, G4, V5, T6), in α1-helix (residues D9, V11-V14, K19-R21), β2- and β3-strands (residues L40, Q46, A52, Q54, L55), α3–helix (residues D66, T69, S70), β4- and β5-strands (residues T88, L99-F101, F103), α4–helix (residues K114, I116, S119, S120, D122, A23, I124, K125, K127), the 3_{10} helix (D141), and loop residues (D43, K44, V57, T129, and I142) (Figure 5.4).

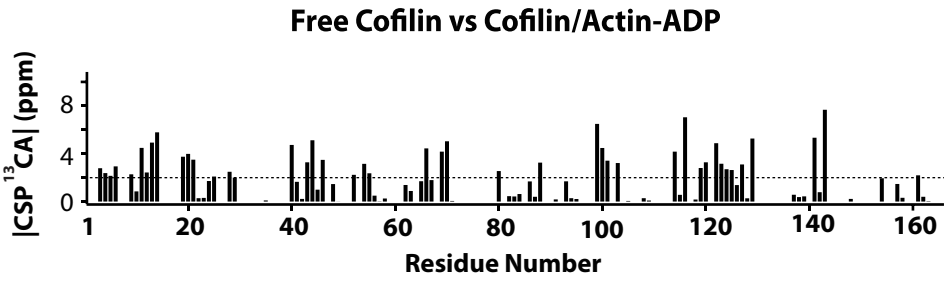

Figure 5.4: Chemical shift perturbations between free cofilin (solution NMR) and cofilin/F-actin-ADP for Cα backbone chemical shifts. Plotted are the chemical shift perturbations as a function of residue number for cofilin sequence.

Chemical shift perturbations of cofilin that occur upon binding of G-actin as reported by Pope et al.[8], show agreement with chemical shift perturbations exhibited in our data for α4–helix residues K114, I116, I124, K125, and K127. Chemical shift perturbations in other residues appear to be specific for F-actin binding. Interestingly, several residues that were reported to show strong G-actin induced chemical shift perturbations by Pope et al.[8] exhibit very small changes or the corresponding peaks are not present in our data. For example, residues V137 and G139, exhibit less than 1 ppm chemical shift perturbations in the MAS NMR spectra of cofilin/F-actin complex albeit large changes were observed upon cofilin binding to G-actin.

Chemical shift perturbation analysis between a protein in complex (cofilin/F-actin) and a free protein (cofilin) generally presents a straightforward way to identify residues interacting at the interface of two biomolecules. However, chemical shift perturbations not only arise from direct interactions between binding partners but can

also be caused by environmental effects such as interactions with solvent and allosteric effects. To distinguish the residues constituting the intermolecular interface formed by cofilin with F-actin from those undergoing allosteric changes upon binding, we employed double REDOR (dREDOR) filtered experiments.[9]

5.3.2 Cofilin-G/F-Actin-ADP Binding Site

The dREDOR-based spectra contain peaks that belong exclusively to the atoms on the U-^{13}C,^{15}N-labeled cofilin that form the intermolecular interface with actin. To perform residue assignments of cofilin residues at the interface, this experiment is implemented as a 2D dREDOR-CORD correlation.

The dREDOR-based measurements revealed the F-actin binding sites on the cofilin surface to an unprecedented level of detail within 8Å. Specifically, the data indicate that the F-actin binding site is comprised of N-terminus residues (S3, G4, and V6) and α4–helix (residues M115 and I116)(Figure 5.5a). However, the entire actin binding surface of the α4–helix appears to be shifted towards the C-terminus compared to the interface in the crystal structure of G-actin with an ADF/cofilin homology domain represented by the C-terminal domain of twinfilin.[10] Residues A123, I124, K127, and T129 at the C-terminal part on the α4–helix, which were not reported to be part of the interface of the G-actin/twinfilin interface, are part of the cofilin/F-actin interface in the complex. These α4–helix residues were also found to be essential for cofilin function *in vivo* by site mutagenesis studies of yeast cofilin[11], solution NMR studies[8], and G-actin binding in synchrotron oxidation experiments.[12]

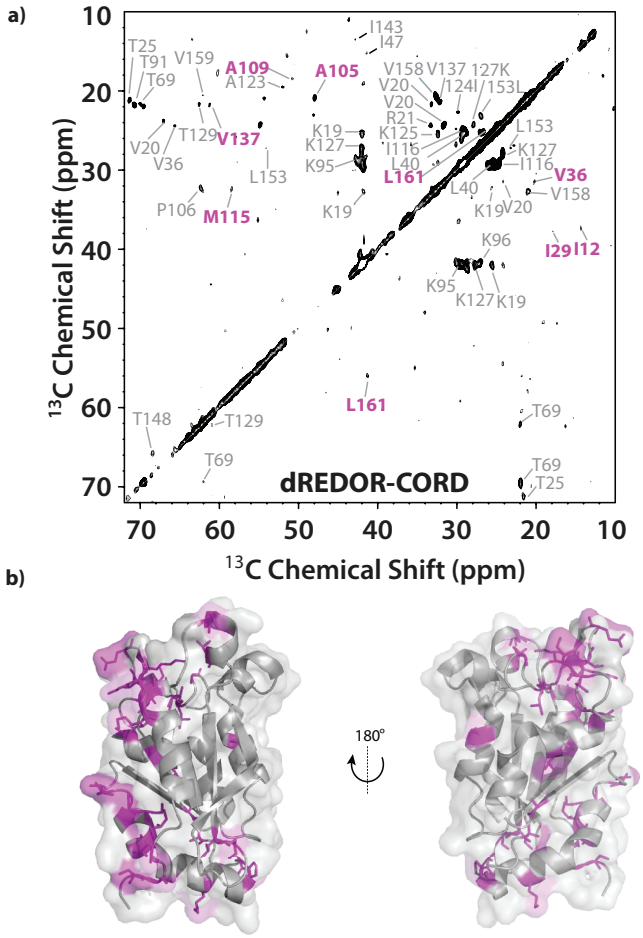

Figure 5.5: (a) Intermolecular interface of human cofilin-2 assembled with polymerized F-actin-ADP. 2D ^{13}C-^{13}C correlation dREDOR-CORD spectrum for U-^{13}C, ^{15}N-cofilin/F-actin ADP complex. Residues constituting the corresponding molecular interface are labeled in the spectrum. (b) 3D solution NMR structure of cofilin-2 (PDB: 1Q8G). Residues present in dREDOR-CORD spectrum are colored in magenta.

5.3.3 Cofilin/F-Actin-ADP Binding Site

To date, the current model for the cofilin/F-actin interface is developed on the basis of cryo-EM studies of human cofilin-2 (PDB: 1Q8G)(Figure 5.6b) and rabbit skeletal actin (PDB: 2BTF). This structure was solved to 9 Å resolution. Our dREDOR data showed excellent agreement with the cryo-EM data in three major regions of F-actin binding (Figure 5.6a). The first was defined as residues 19-21 (also present in cryo-EM study) and 24-26. Loop residues 24-32 are present in vertebrates but not in yeast or plant cofilins. This loop contains a nuclear localization signal (NLS) essential for active translocation of G-actin-cofilin complexes to the nucleus.[13,14] It has been reported that the phosphorylation of S23 or S24 reduces the ability of cofilin to bind F-actin and to modify actin dynamics *in vitro* and *in vivo*.[15] The ability of the 24-32 loop to interact with F-actin but not G-actin may suggest a possible mechanism of discriminative recognition of free cofilin and actin-cofilin complexes by nuclear importins.

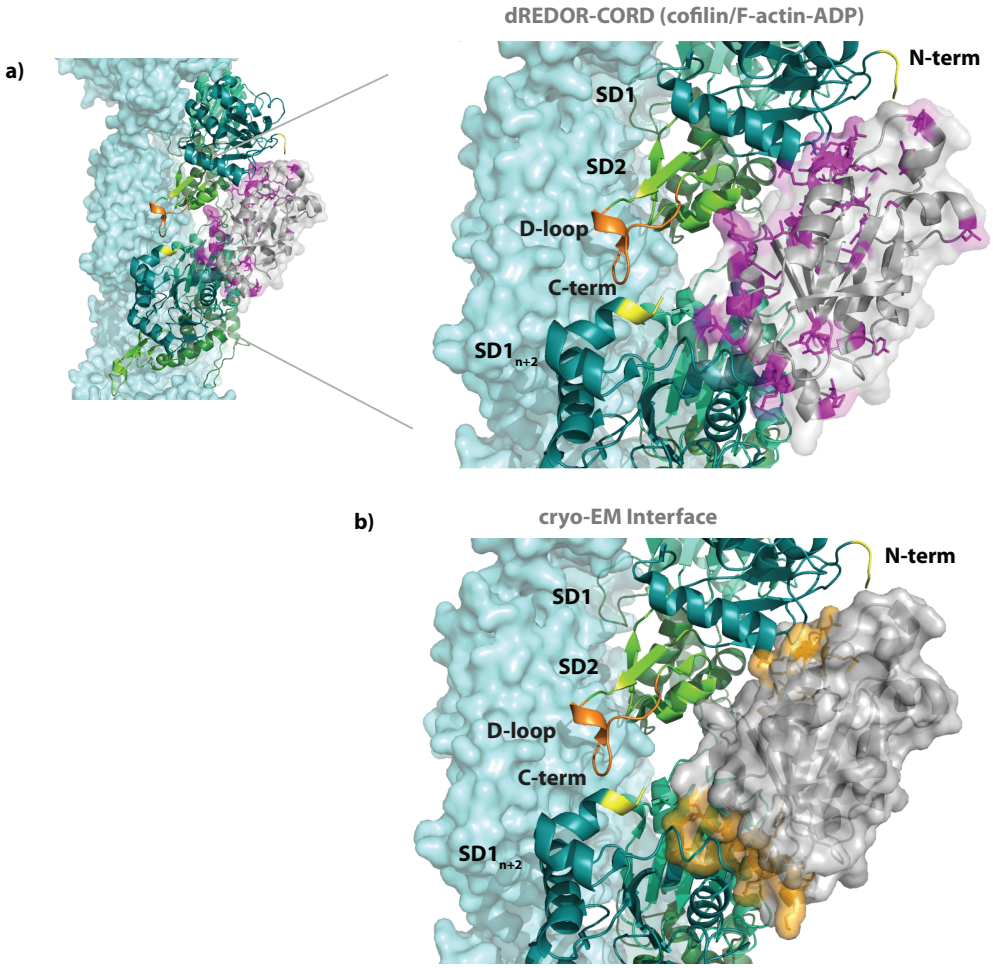

Figure 5.6: (a) Structure of F-actin (cyan) decorated with cofilin (gray) determined by cryo-EM (PDB: 3J0S).[1] Two adjacent protomers of actin are shown as cartoons. Interface residues (red) S3, G4, V6, I12, K19, V20, R21, T25, I29, V36, L40, S41, T63, T69, T91, E93, S94, K95, K96, L99, V100, A105, A109, M115, I116, A123, I124, K127, T129, V137, T148, L153, V158, V159, L161 and G163 obtained from dREDOR-CORD MAS NMR experiments of human cofilin-2/F-actin-ADP are shown in magenta. Subdomains of actin protomers (n and n+1) are colored in teal (SD1, SD_{n+2}), green (SD2), and cyan (SD3, SD4). DNase binding loop (orange), N-terminus (yellow) and C-terminus (yellow) are indicated on the actin structure. (b) Interface residues determined from cryo-EM studies mapped onto cofilin structure. Residues M1-V5, K19-R21, S94-D98, K112-S119 and G154-V158 are shown in orange.

The second region was composed of residues from the loop connecting β4-β5 strands and the β5 strand (91, 93-96 and 99-100). That these residues comprise the intermolecular interface with F-actin agrees with cryo-EM results revealing residues 94-98 to be at the interface. Residues, 153, 157-160 and 163 at the C-terminal end of cofilin form a third F-actin binding site. In the cryo-EM structure, residues 154-158 were also seen to be at the interface. Pope et al. reported that this region defines a major structural difference between cofilin and ADF in a stronger binding to F-actin due to a tighter folding of this region.[8]

Apart from these well-defined regions of dREDOR determined interface residues, dREDOR spectra revealed residues that did not appear to be on the surface of the intermolecular interface of actin according to cryo-EM data. For example, residues T63, T69, and S70 appeared to be located on the opposite side of the actin-binding sites.

As illustrated in Figure 5.7, many residues that experience chemical shift perturbations are also present in the 2D dREDOR-CORD spectrum. However, there are a number residues exhibiting chemical shift perturbations that do not appear in the dREDOR spectrum. These residues experience allosteric effects due to the conformational changes upon interaction with F-actin but do not belong to the intermolecular interface.

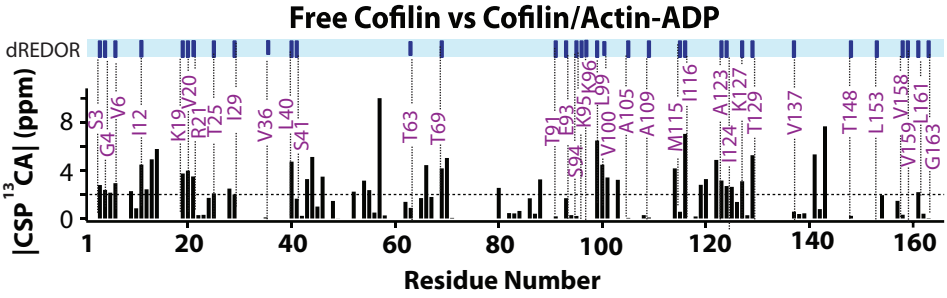

Figure 5.7: Chemical shift perturbations between free cofilin and cofilin/F-actin-ADP as a function of cofilin residue number. Residues present in dREDOR-CORD experiments of cofilin/F-actin-ADP are shown with blue bars above the plot and labeled in purple.

5.4 Chemical Shift Perturbations in Cofilin Between Two Nucleotide States

Binding of BeFx to ADP-actin mimics an ADP-Pi state of the filament characterized by low affinity to cofilin. To investigate the unique interface that cofilin forms with F-actin-ADP-BeFx and F-actin-ADP, chemical shift perturbations in cofilin/F-actin-ADP vs. cofilin/F-acin-ADP-BeFx were analyzed. Chemical shift changes were compared for homo- and heteronuclear datasets, NCA, NCACX and CORD. The concentrations used in this study (μM of cofilin and μM of actin) the proteins form a stable complex, that has been pelleted and analyzed by MAS NMR at 19.96 T (Figure 5.8). Surprisingly the resolution of this sample is higher than that of the U-^{13}C, ^{15}N-cofilin in complex with F-actin-ADP, potentially reflecting lower conformational entropy of the complex under these conditions (i.e., the actin filaments with binding sites accessible to cofilin are conformationally homogeneous in the BeFx-ADP bound state). Although both ADP- and BeFx-ADP-actin samples exhibited similar sensitivity in heteronuclear NCA spectra (Figure 5.11a) for the majority of resolved residues, the peak intensities of G4, G61 and S119 residues in the

ADP-BeFx-actin complex were higher; Improved sensitivity and resolution for this sample enabled resonances A2, S24, K127, and L153 to be assigned.

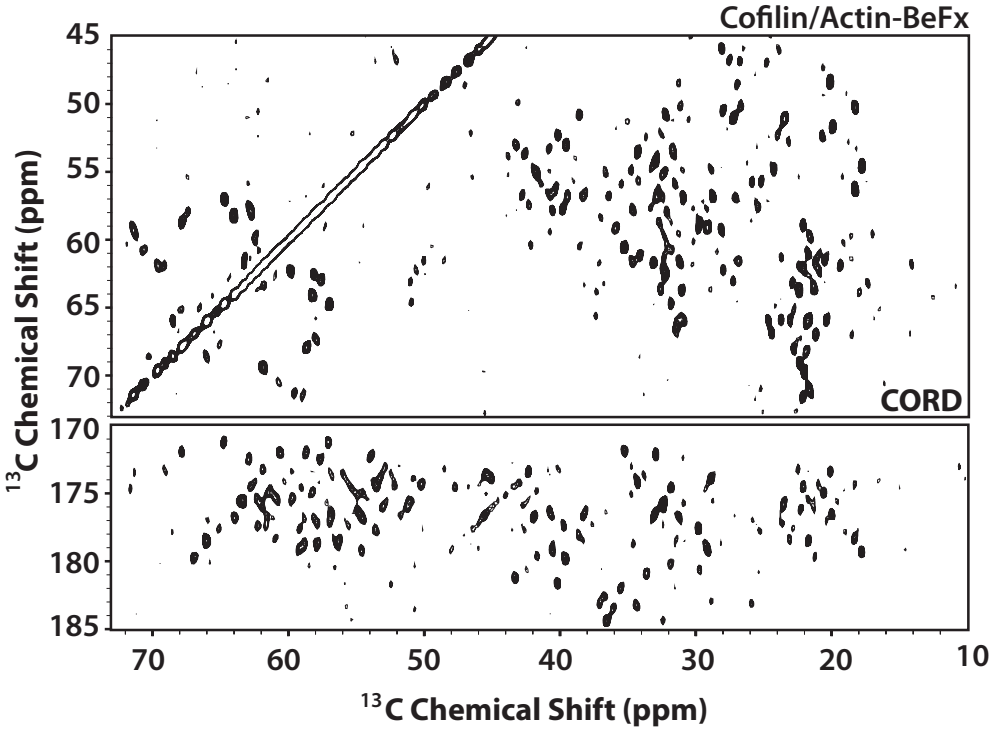

Figure 5.8: The aliphatic and carbonyl regions of the CORD spectrum of cofilin/F-actin-ADP-BeFx acquired at 19.96 T.

Interestingly, chemical shift perturbations were observed for backbone and aliphatic resonances between different nucleotide states of F-actin (Figure 5.9 and Figure 5.10) in homonuclear and heteronuclear datasets. Of the 116 residues assigned in U-^{13}C, ^{15}N cofilin/F-actin-ADP spectra, 20 residues show chemical shift perturbations in ^{13}C-^{13}C correlation spectra (Figure 5.11e-h) or NCA (Figure 5.11c) and NCACX datasets (Figure 5.11b,d) (exemplified by A52 C^{α}-C^{β} resonances, V5 aliphatic (C^{α}-$C^{\gamma 1}$) chemical shifts. In Figure 5.11g, the chemical shift perturbations in

the CORD spectrum associated with the A52 C^{α}-C^{β} resonances are illustrated. K19 (Figure 5.11b) and V157 (Figure 5.11c) show slightly smaller chemical shift perturbations in heteronuclear NCA/NCACX spectra compared to those observed for V5 and A52.

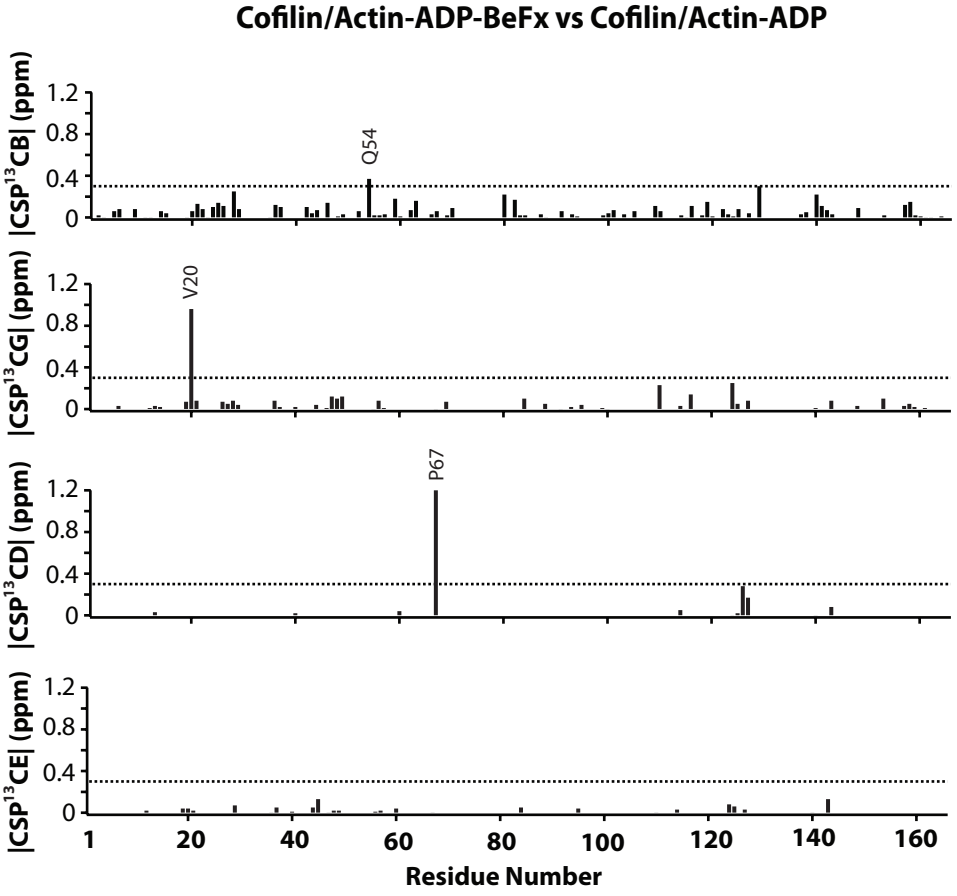

Figure 5.9: Chemical shift perturbations (CSP) between cofilin/F-actin-ADP and cofilin/F-actin-ADP-BeFx complexes observed in 2D NCACX spectra, plotted for the assigned residues. Residues exhibiting CSPs greater than 0.3 ppm are labeled; these large CSPs indicate significant conformational differences between the two-nucleotide states.

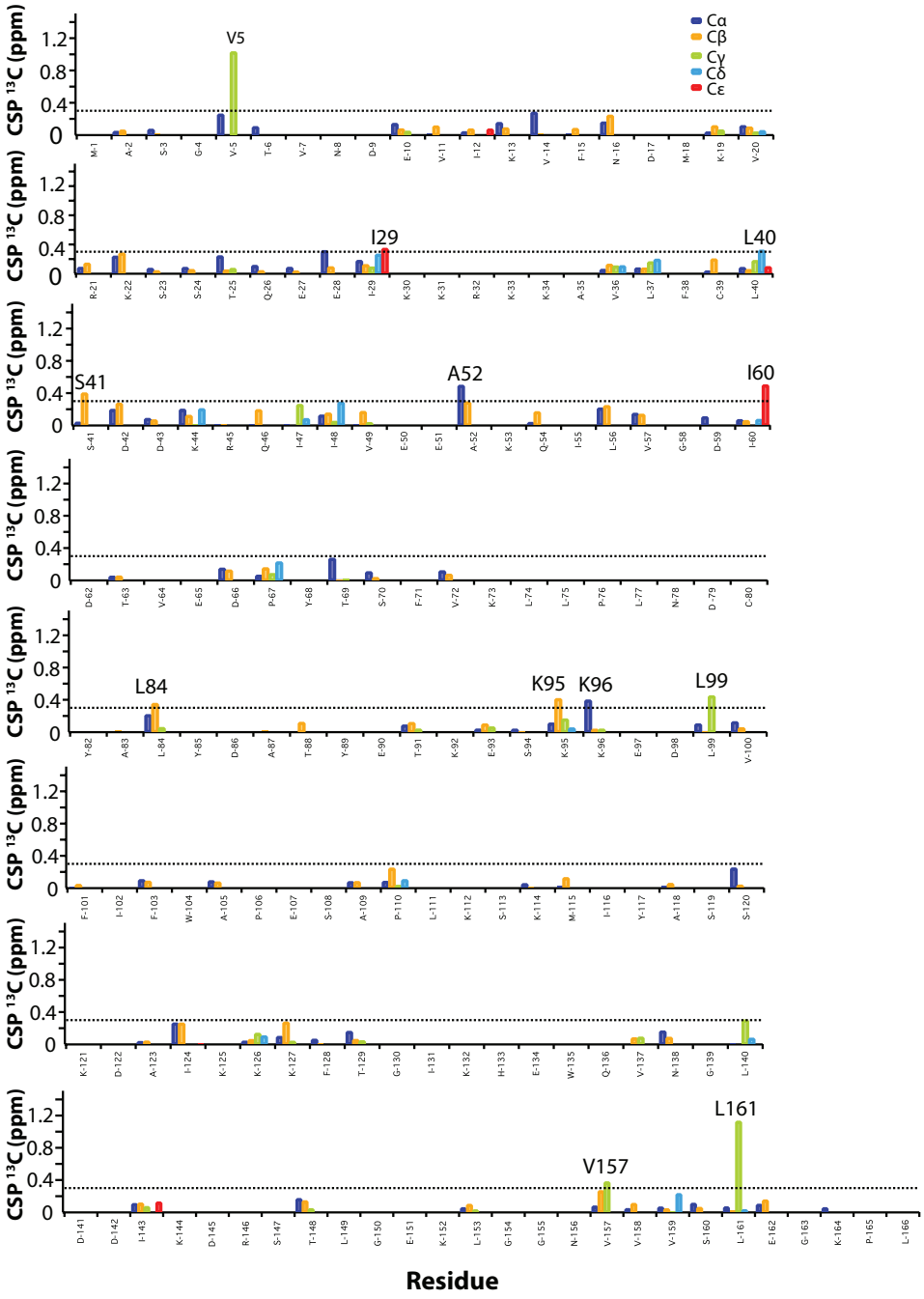

Figure 5.10: Chemical shift perturbations (CSPs) between cofilin/actin-ADP and cofilin/F-actin-ADP-BeFx observed in CORD MAS NMR spectrum and plotted for the assigned residues. Residues exhibiting CSPs greater than 0.3 ppm are labeled; these large CSPs indicate significant conformational differences between the two nucleotide states.

Comparisons of chemical shifts for the backbone nitrogen and carbon atoms (Figure 5.11i and Figure 511j, respectively) for the cofilin/F-actin-ADP vs cofilin/F-actin-ADP-BeFx complex reveals that for a number of residues, differences of 0.3 ppm or greater are observed. The backbone CSPs are associated with residues G4, T6 at the N-terminus (G-site); K19, V20, T25, I29 in the α1 and α2 helices, L40, S41 at the tip of β1; K95, K96, L99 in the long loop between β3 and β4, M115, S119, I124 in the α4 helix (G-site); V137 at the tip of β5, and residue V157, V158 near the C-terminus. The magnitude of these chemical shifts perturbations are significantly smaller compared to that between free cofilin and bound cofilin.

In addition to chemical shift perturbations, peak intensities in heteronuclear NCA spectra were used to study differences between the interactions of cofilin with the two different nucleotide states of F-actin. Relative ratios of sensitivity-normalized peak intensities were analyzed for all resolved peaks detected in the heteronuclear NCA spectra and plotted for each residue in Figures 5.12. The peak intensities for each residue were normalized using an isolated G163 residue present in the spectrum (normalizing to V72 or S70 peak intensities yielded similar results). As shown in Figure 5.12, sixteen residues exemplified a difference in relative peak intensity greater than 20% for cofilin/F-actin-ADP as compared to cofilin/F-actin-ADP-BeFx spectra. Surprisingly, only three residues with differences in peak intensities (I29 and K125) or both peak intensity and chemical shift perturbations (V5) belong to the intermolecular interface with actin when mapped on the cryo-EM structure of the F-actin cofilin complex.

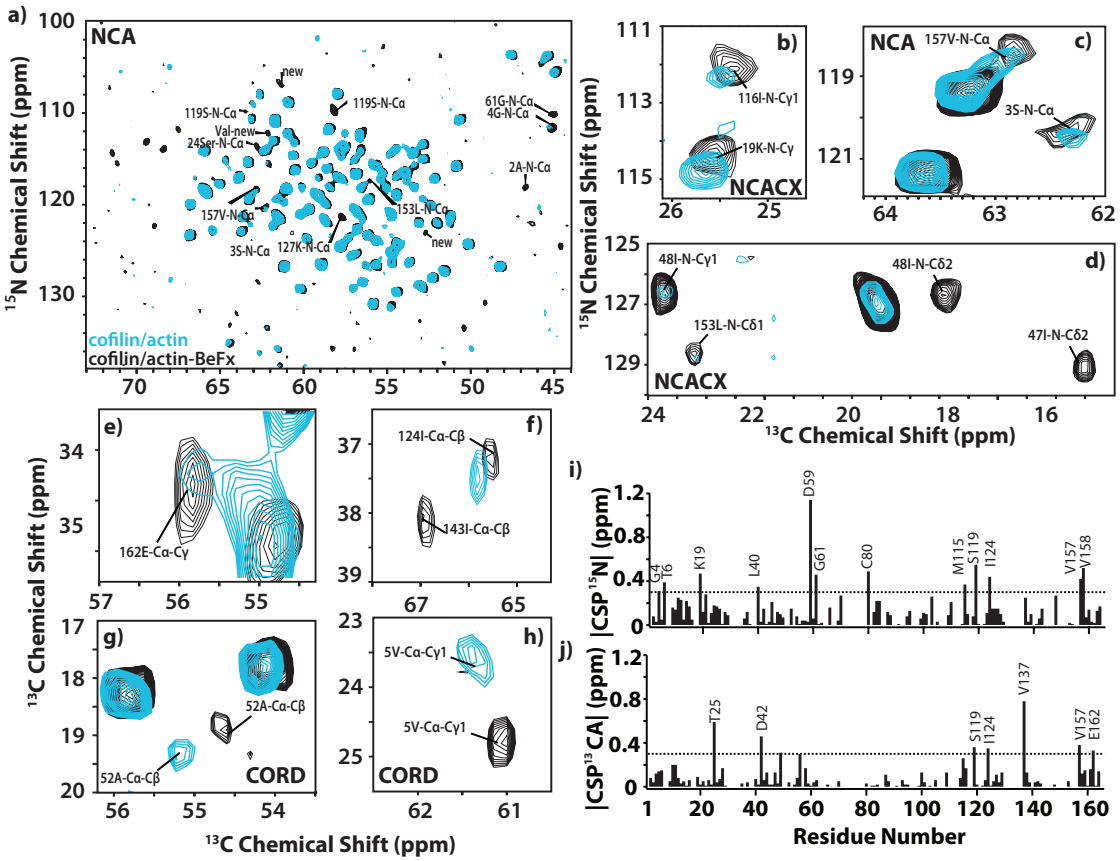

Figure 5.11: (a) Overlay of 2D NCA MAS NMR spectra of cofilin-2/F-actin-ADP (light blue contours) and cofilin-2/F-actin-ADP-BeFx (black). Expansions of 2D NCACX (b), NCA (c) and NCACX (d) spectra for selected residues showing chemical shift perturbations or intensity changes for cofilin-2/F-actin-ADP (light blue contours) and cofilin-2/F-actin-ADP-BeFx (black contours). (e-h) Overlay of the selected expansions of CORD spectra of cofilin-2/F-actin-ADP (light blue contours) and cofilin-2/F-actin-ADP-BeFx (black contours) showing ^{13}C chemical shift perturbations. (i-j) Chemical shift perturbations (CSP) between cofilin/F-actin-ADP and cofilin/F-actin-ADP-BeFx complexes observed in 2D NCACX spectra, plotted for the assigned residues. Residues exhibiting CSP greater than 0.3 ppm are labeled; these large CSP indicate pronounced conformational differences between the two-nucleotide states.

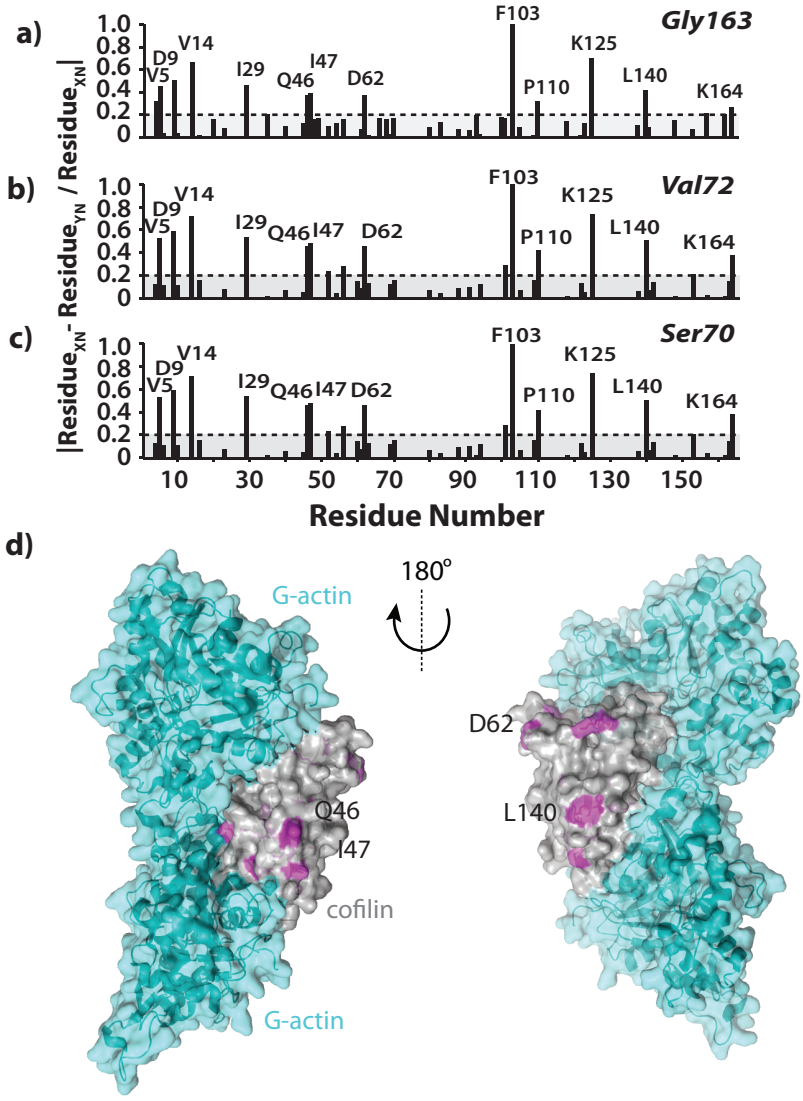

Figure 5.12: Relative ratio of normalized peak intensities corresponding to resolved signals in the NCA spectra of cofilin-2/F-actin-ADP and cofilin-2/F-actin-ADP-BeFx. The intensities were normalized with respect to G163 (a) V72 (b) and S70 (c). These rigid residues do not undergo intensity changes in the spectra. (d) Residues that experience changes in relative intensity above 20% (magenta) are mapped on surface display of cryo-EM cofilin (gray)/actin (cyan) structure (PDB: 3J0S).

5.5 Cofilin/F-Actin-ADP-BeFx Binding

The 2D dREDOR-CORD spectrum of cofilin/actin-ADP complex obtained in the presence of BeFx is shown in Figure 5.13a. The residues yielding cross peaks and therefore constituting the intermolecular cofilin/actin interface, are summarized in Fig. 13b. In agreement with the replacement of BeFx by cofilin, the majority of the cross peaks belong to the same cofilin residues as in the complex with actin-ADP (Figure 5.14a). However, there are several differences where signals appear only in one of the complexes: Q46, S119, S120 are found only in the presence of BeFx, whereas I12, I29, V36, A105, A109, V137 were detected only in ADP-complex in the absence of BeFx (Figure 5.14c). A summary of residues that appear in the dREDOR spectra for cofilin/F-actin-ADP and cofilin/F-actin-ADP-BeFx is given in Table 5.1.

The data revealed the presence of more longitudinal contacts between cofilin and adjacent actin-ADP-BeFx protomers. This result supports prior biochemical evidence that in its ADP-bound state (where the Pi has been released after ATP hydrolysis) F-actin is less stable and has more internal flexibility and lower persistence length relative to ATP and ADP-Pi actin filaments.

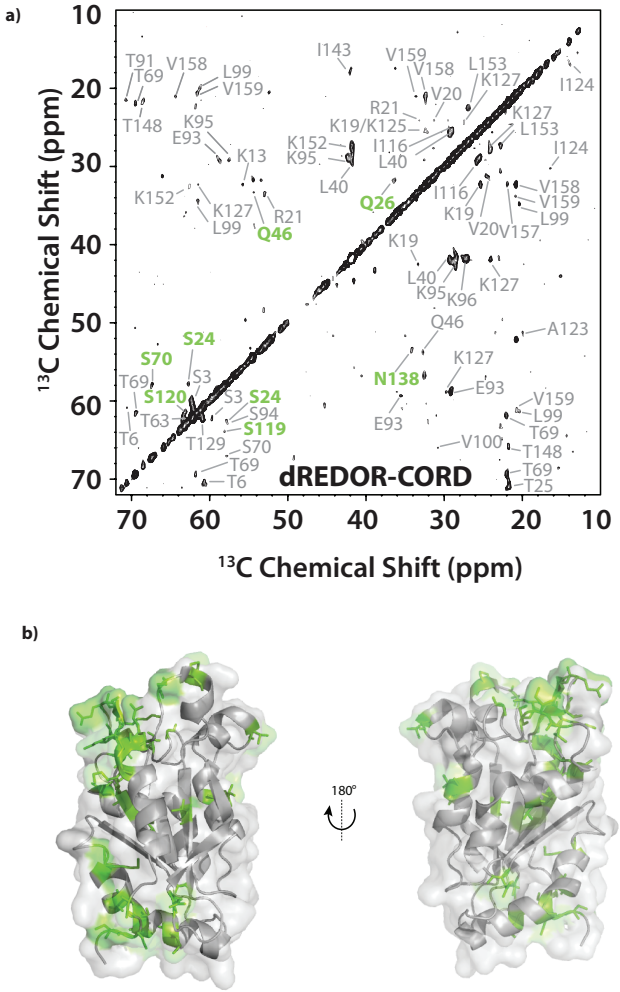

Figure 5.13: (a) Intermolecular interface of human cofilin-2 assembled with polymerized F-actin-ADP-BeFx. 2D ^{13}C-^{13}C correlation dREDOR-CORD spectrum for U-^{13}C, ^{15}N-cofilin/F-actin ADP complex. Residues constituting the corresponding molecular interface are labeled in the spectrum. (b) 3D solution NMR structure of cofilin-2 (PDB: 1Q8G). Residues present in dREDOR-CORD spectrum are colored in green.

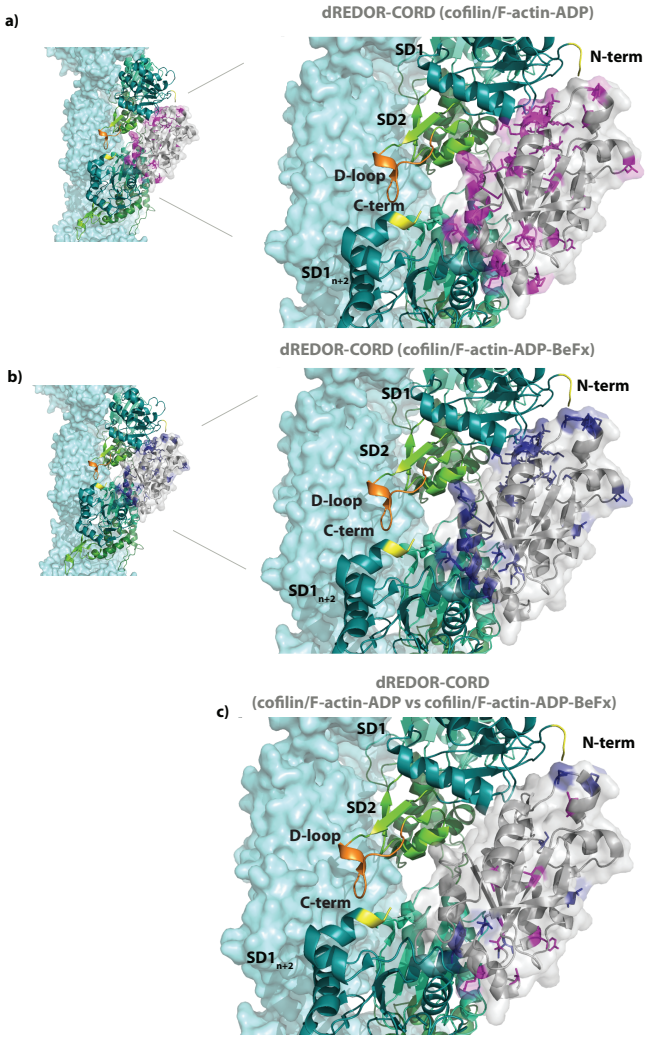

Figure 5.14: Structure of F-actin (cyan) decorated with cofilin (gray) determined by cryo-EM (PDB: 3J0S). Two adjacent protomers of actin are shown as cartoons. (a) Interface residues (magenta) obtained from dREDOR-CORD MAS NMR experiments of human cofilin-2/F-actin-ADP are shown in magenta. (b) Interface residues (dark blue) obtained from dREDOR-CORD MAS NMR of human cofilin-2/F-actin-ADP-BeFx. (c) Residues detected in dREDOR-CORD experiments and present only in actin-ADP (magenta) or actin-ADP-BeFx (dark blue) are mapped onto cofilin structure. (f) Chemical shift perturbations (purple) between cofilin/actin-ADP and cofilin/actin-ADP-BeFx are mapped onto cofilin structure.

Table 5.1: Summary table of U-^{13}C, ^{15}N-cofilin-2/actin-ADP resonance assignments by solution and MAS solid-state NMR experiments. Residues experiencing chemical shift perturbations/peak intensity changes in NCA spectra and/or those present in dREDOR-CORD spectra are shown. The residues found in dREDOR-CORD spectra constitute intermolecular interface with actin. The residues with perturbed chemical shifts or peak intensities are either part of intermolecular interface with actin or undergo allosteric conformational changes.

		Resonance Assignments		Residues Undergoing Conformational Changes Upon Binding to Actin-ADP-BeFx			
Residue Number	Residue Type	Solution NMR Experiments	Solid-State NMR Experiments	dREDOR-CORD (cofilin/actin-ADP)	dREDOR-CORD (cofilin/actin-ADP-BeFx)	Chemical Shift Perturbations (actin-ADP vs actin-ADP-BeFx)	NCA Peak Intensity Perturbat-ions: S/N (>20% rel. ratio)
1	MET						
2	ALA		✓				
3	SER	✓	✓	✓	✓		
4	GLY	✓	✓	✓	✓	✓	✓
5	VAL	✓	✓			✓	✓
6	THR	✓	✓	✓	✓	✓	
7	VAL	✓					
8	ASN	✓					
9	ASP	✓	✓				✓
10	GLU	✓	✓				
11	VAL	✓	✓				
12	ILE	✓	✓	✓			
13	LYS	✓	✓				
14	VAL	✓	✓				✓
15	PHE		✓				
16	ASN		✓				
17	ASP		✓				
18	MET						
19	LYS	✓	✓	✓	✓	✓	
20	VAL	✓	✓	✓	✓	✓	
21	ARG	✓	✓	✓	✓		
22	LYS	✓	✓				
23	SER	✓	✓				
24	SER	✓	✓		✓		
25	THR	✓	✓	✓	✓	✓	
26	GLN		✓		✓		
27	GLU		✓				
28	GLU	✓	✓				
29	ILE	✓	✓	✓		✓	✓
30	LYS	✓					
31	LYS						
32	ARG	✓					
33	LYS	✓					
34	LYS	✓					
35	ALA	✓	✓				
36	VAL		✓	✓			
37	LEU		✓				
38	PHE						
39	CYS		✓				

40	LEU	✓	✓	✓	✓	✓	
41	SER	✓	✓	✓		✓	
42	ASP	✓	✓			✓	
43	ASP	✓	✓				
44	LYS	✓	✓				
45	ARG	✓	✓				
46	GLN	✓	✓		✓		✓
47	ILE		✓				✓
48	ILE	✓	✓				
49	VAL	✓	✓				
50	GLU	✓					
51	GLU	✓					
52	ALA	✓	✓			✓	✓
53	LYS	✓					
54	GLN	✓	✓			✓	
55	ILE	✓	✓				
56	LEU	✓	✓				✓
57	VAL	✓	✓				
58	GLY	✓	✓				
59	ASP		✓			✓	
60	ILE		✓			✓	
61	GLY		✓			✓	
62	ASP	✓	✓				✓
63	THR	✓	✓	✓	✓		
64	VAL	✓					
65	GLU	✓	✓				
66	ASP	✓	✓				
67	PRO	✓	✓			✓	
68	TYR	✓	✓				
69	THR	✓	✓	✓	✓		
70	SER	✓	✓		✓		
71	PHE	✓	✓				
72	VAL	✓	✓				
73	LYS	✓					
74	LEU						
75	LEU	✓					
76	PRO						
77	LEU						
78	ASN	✓					
79	ASP	✓					
80	CYS	✓	✓			✓	
81	ARG	✓					
82	TYR	✓	✓				
83	ALA	✓	✓				
84	LEU	✓	✓			✓	
85	TYR	✓					
86	ASP	✓	✓				
87	ALA	✓	✓				
88	THR	✓	✓				
89	TYR	✓					
90	GLU	✓					
91	THR	✓	✓	✓	✓		
92	LYS	✓					
93	GLU	✓	✓	✓	✓		
94	SER	✓	✓	✓	✓		
95	LYS	✓	✓	✓	✓	✓	
96	LYS	✓		✓	✓	✓	
97	GLU	✓					
98	ASP	✓					
99	LEU	✓	✓	✓	✓	✓	
100	VAL	✓	✓	✓	✓		

101	PHE	✓	✓				✓
102	ILE	✓					
103	PHE	✓	✓				✓
104	TRP	✓					
105	ALA	✓	✓	✓			
106	PRO						
107	GLU	✓					
108	SER	✓	✓				
109	ALA	✓	✓	✓			
110	PRO						✓
111	LEU	✓					
112	LYS	✓					
113	SER	✓					
114	LYS	✓	✓				
115	MET	✓	✓	✓		✓	
116	ILE	✓	✓	✓	✓		
117	TYR	✓					
118	ALA	✓	✓				
119	SER	✓	✓		✓	✓	
120	SER	✓	✓		✓		
121	LYS	✓					
122	ASP	✓	✓				
123	ALA	✓	✓	✓	✓		
124	ILE	✓	✓	✓	✓	✓	
125	LYS	✓	✓				✓
126	LYS	✓	✓				
127	LYS	✓	✓	✓	✓		
128	PHE	✓	✓				
129	THR	✓	✓	✓	✓		
130	GLY	✓					
131	ILE	✓					
132	LYS	✓					
133	HIS	✓					
134	GLU	✓					
135	TRP	✓					
136	GLN	✓					
137	VAL	✓	✓	✓		✓	
138	ASN	✓	✓		✓		
139	GLY	✓	✓				
140	LEU	✓	✓				✓
141	ASP	✓	✓				
142	ASP	✓	✓				
143	ILE	✓	✓				
144	LYS	✓					
145	ASP	✓					
146	ARG	✓					
147	SER	✓					
148	THR	✓	✓	✓	✓		
149	LEU	✓	✓				
150	GLY	✓					
151	GLU						
152	LYS		✓				
153	LEU		✓	✓	✓		
154	GLY	✓	✓				
155	GLY	✓					
156	ASN	✓					
157	VAL	✓	✓		✓	✓	
158	VAL	✓	✓	✓	✓	✓	
159	VAL		✓	✓	✓		
160	SER		✓		✓		
161	LEU	✓	✓	✓		✓	

162	GLU	✓	✓			✓	
163	GLY	✓	✓	✓	✓		
164	LYS		✓				✓
165	PRO						
166	LEU						

5.6 Conclusions

In this work, we determined the interfaces formed by cofilin bound with two different nucleotide states of F-actin, F-actin-ADP-BeFx (F-actin-ADP-Pi mimic) and F-actin-ADP. We demonstrate that MAS NMR spectra of cofilin/actin assemblies exhibit outstanding resolution, permitting their structural analysis at atomic resolution and with unprecedented level of detail. The study presented here provides clues about the regulation of the cofilin / F-actin interactions by the nucleotide and opens doors for atomic-resolution characterization of assemblies formed by F-actin with other actin-binding proteins.

Our work also establishes that cofilin/actin-ADP-BeFx is a more stable and less dynamic complex compared to cofilin/actin-ADP. First, we observed that cofilin bound to F-actin-ADP-BeFx exhibits remarkably narrow lines in the dipolar-based MAS NMR spectra. This observation suggests that cofilin is more flexible and/or less conformationally homogeneous in complex with F-actin-ADP, which is consistent with a recent study, where cofilin was found to induce disorders and flexibility in actin's SD2. Second, our data revealed the presence of more longitudinal contacts between cofilin and adjacent actin-ADP-BeFx protomers. This result supports prior biochemical evidence that in its ADP-bound state (where the Pi has been released after ATP hydrolysis) F-actin is less stable and has more internal flexibility and lower persistence length relative to ATP and ADP-Pi actin filaments. Moreover, it is recognized that binding of cofilin to actin is primarily driven by positive entropy

changes. Thus higher structural rigidity of ADP-BeFx actin correlates well with its lower affinity to cofilin. We therefore conclude, on the basis of our current data and previous findings summarized above, that the extent of the disorder and conformational flexibility of cofilin in complexes with actin is dependent on the F-actin's nucleotide state. We speculate that such varied degree of conformational flexibility may provide a mechanism for cofilin's regulation of actin polymerization dynamics in different nucleotide states.

REFERENCES

(1) Galkin, V. E.; Orlova, A.; Kudryashov, D. S.; Solodukhin, A.; Reisler, E.; Schroder, G. F.; Egelman, E. H. *Proc. Natl. Acad. Sci. USA* **2011**, *108*, 20568.

(2) McGough, A.; Pope, B.; Chiu, W.; Weeds, A. *J. Cell Biol.* **1997**, *138*, 771.

(3) Dominguez, R. *Trends Biochem. Sci.* **2004**, *29*, 572.

(4) Levitsky, D. I.; Pivovarova, A. V.; Mikhailova, V. V.; Nikolaeva, O. P. *FEBS J.* **2008**, *275*, 4280.

(5) Isambert, H.; Venier, P.; Maggs, A. C.; Fattoum, A.; Kassab, R.; Pantaloni, D.; Carlier, M. F. *J. Biol. Chem.* **1995**, *270*, 11437.

(6) Weingarth, M.; Baldus, M. *Acc. Chem. Res.* **2013**, *46*, 2037.

(7) Yang, J.; Tasayco, M. L.; Polenova, T. *J. Am. Chem. Soc.* **2008**, *130*, 5798.

(8) Pope, B. J.; Zierler-Gould, K. M.; Kuhne, R.; Weeds, A. G.; Ball, L. J. *J. Biol. Chem.* **2004**, *279*, 4840.

(9) Yan, S.; Guo, C.; Hou, G.; Zhang, H.; Lu, X.; Williams, J. C.; Polenova, T. *Proc. Natl. Acad. Sci. USA* **2015**, *112*, 14611.

(10) Paavilainen, V. O.; Oksanen, E.; Goldman, A.; Lappalainen, P. *J. Cell Biol.* **2008**, *182*, 51.

(11) Lappalainen, P.; Fedorov, E. V.; Fedorov, A. A.; Almo, S. C.; Drubin, D. G. *EMBO J.* **1997**, *16*, 5520.

(12) Guan, J. Q.; Vorobiev, S.; Almo, S. C.; Chance, M. R. *Biochemistry* **2002**, *41*, 5765.

(13) Munsie, L. N.; Truant, R. *Bioarchitecture* **2012**, *2*, 204.

(14) Munsie, L. N.; Desmond, C. R.; Truant, R. *J. Cell Sci.* **2012**, *125*, 3977.

(15) Sakuma, M.; Shirai, Y.; Yoshino, K. *Mol. Biol. Cell.* **2012**, *23*, 3707.